

DESY 99-102
July 1999

Measurement of the Spin-Density Matrix Elements in Exclusive Electroproduction of ρ^0 Mesons at HERA

ZEUS Collaboration

Abstract

Exclusive electroproduction of ρ^0 mesons has been measured using the ZEUS detector at HERA in two Q^2 ranges, $0.25 < Q^2 < 0.85 \text{ GeV}^2$ and $3 < Q^2 < 30 \text{ GeV}^2$. The low- Q^2 data span the range $20 < W < 90 \text{ GeV}$; the high- Q^2 data cover the $40 < W < 120 \text{ GeV}$ interval. Both samples extend up to four-momentum transfers of $|t| = 0.6 \text{ GeV}^2$. The distribution in the azimuthal angle between the positron scattering plane and the ρ^0 production plane shows a small but significant violation of s -channel helicity conservation, corresponding to the production of longitudinally polarised (i.e. helicity zero) ρ^0 mesons from transverse photons. Measurements of the 15 combinations of spin-density matrix elements which completely define the angular distributions are presented and discussed.

The ZEUS Collaboration

J. Breitweg, S. Chekanov, M. Derrick, D. Krakauer, S. Magill, B. Musgrave, A. Pellegrino,
J. Repond, R. Staneck, R. Yoshida

Argonne National Laboratory, Argonne, IL, USA ^p

M.C.K. Mattingly

Andrews University, Berrien Springs, MI, USA

G. Abbiendi, F. Anselmo, P. Antonioli, G. Bari, M. Basile, L. Bellagamba, D. Boscherini¹,
A. Bruni, G. Bruni, G. Cara Romeo, G. Castellini², L. Cifarelli³, F. Cindolo, A. Contin,
N. Coppola, M. Corradi, S. De Pasquale, P. Giusti, G. Iacobucci⁴, G. Laurenti, G. Levi,
A. Margotti, T. Massam, R. Nania, F. Palmonari, A. Pesci, A. Polini, G. Sartorelli,
Y. Zamora Garcia⁵, A. Zichichi

University and INFN Bologna, Bologna, Italy ^f

C. Amelung, A. Bornheim, I. Brock, K. Coböken, J. Crittenden, R. Deffner, M. Eckert⁶,
H. Hartmann, K. Heinloth, E. Hilger, H.-P. Jakob, A. Kappes, U.F. Katz, R. Kerger,
E. Paul, J. Rautenberg⁷,

H. Schnurbusch, A. Stifutkin, J. Tandler, A. Weber, H. Wieber
Physikalisches Institut der Universität Bonn, Bonn, Germany ^c

D.S. Bailey, O. Barret, W.N. Cottingham, B. Foster⁸, G.P. Heath, H.F. Heath, J.D. Mc-
Fall, D. Piccioni, J. Scott, R.J. Tapper

H.H. Wills Physics Laboratory, University of Bristol, Bristol, U.K. ^o

M. Capua, A. Mastroberardino, M. Schioppa, G. Susinno

Calabria University, Physics Dept. and INFN, Cosenza, Italy ^f

H.Y. Jeoung, J.Y. Kim, J.H. Lee, I.T. Lim, K.J. Ma, M.Y. Pac⁹

Chonnam National University, Kwangju, Korea ^h

A. Caldwell, W. Liu, X. Liu, B. Mellado, J.A. Parsons, S. Ritz¹⁰, R. Sacchi, S. Sampson,
F. Sciulli

Columbia University, Nevis Labs., Irvington on Hudson, N.Y., USA ^q

J. Chwastowski, A. Eskreys, J. Figiel, K. Klimek, K. Olkiewicz, M.B. Przybycień, P. Stopa,
L. Zawiejski

Inst. of Nuclear Physics, Cracow, Poland ^j

L. Adamczyk¹¹, B. Bednarek, K. Jeleń, D. Kisielewska, A.M. Kowal, T. Kowalski, M. Przy-
bycień,

E. Rulikowska-Zarębska, L. Suszycki, J. Zajac

*Faculty of Physics and Nuclear Techniques, Academy of Mining and Metallurgy, Cracow,
Poland* ^j

Z. Duliński, A. Kotański

Jagellonian Univ., Dept. of Physics, Cracow, Poland ^k

L.A.T. Bauerdick, U. Behrens, J.K. Bienlein, C. Burgard, K. Desler, G. Drews, A. Fox-Murphy, U. Fricke, F. Goebel, P. Göttlicher, R. Graciani, T. Haas, W. Hain, G.F. Hartner, D. Hasell¹², K. Hebbel, K.F. Johnson¹³, M. Kasemann¹⁴, W. Koch, U. Kötz, H. Kowalski, L. Lindemann, B. Löhr, M. Martínez, J. Milewski¹⁵, M. Milite, T. Monteiro¹⁶, M. Moritz, D. Notz, F. Pelucchi, M.C. Petrucci, K. Piotrzkowski, M. Rohde, P.R.B. Saull, A.A. Savin, U. Schneekloth, O. Schwarzer¹⁷, F. Selonke, M. Sievers, S. Stonjek, E. Tassi, G. Wolf, U. Wollmer, C. Youngman, W. Zeuner

Deutsches Elektronen-Synchrotron DESY, Hamburg, Germany

B.D. Burow¹⁸, C. Coldewey, H.J. Grabosch, A. Lopez-Duran Viani, A. Meyer, K. Mönig, S. Schlenstedt, P.B. Straub

DESY Zeuthen, Zeuthen, Germany

G. Barbagli, E. Gallo, P. Pelfer

University and INFN, Florence, Italy^f

G. Maccarrone, L. Votano

INFN, Laboratori Nazionali di Frascati, Frascati, Italy^f

A. Bamberger, S. Eisenhardt¹⁹, P. Markun, H. Raach, S. Wölflle

Fakultät für Physik der Universität Freiburg i.Br., Freiburg i.Br., Germany^c

N.H. Brook²⁰, P.J. Bussey, A.T. Doyle, S.W. Lee, N. Macdonald, G.J. McCance, D.H. Saxon, L.E. Sinclair, I.O. Skillicorn, E. Strickland, R. Waugh

Dept. of Physics and Astronomy, University of Glasgow, Glasgow, U.K.^o

I. Bohnet, N. Gendner, U. Holm, A. Meyer-Larsen, H. Salehi, K. Wick

Hamburg University, I. Institute of Exp. Physics, Hamburg, Germany^c

A. Garfagnini, I. Gialas²¹, L.K. Gladilin²², D. Kçira²³, R. Klanner, E. Lohrmann, G. Poelz, F. Zetsche

Hamburg University, II. Institute of Exp. Physics, Hamburg, Germany^c

T.C. Bacon, J.E. Cole, G. Howell, L. Lamberti²⁴, K.R. Long, D.B. Miller, A. Prinias²⁵, J.K. Sedgbeer, D. Sideris, A.D. Tapper, R. Walker

Imperial College London, High Energy Nuclear Physics Group, London, U.K.^o

U. Mallik, S.M. Wang

University of Iowa, Physics and Astronomy Dept., Iowa City, USA^p

P. Cloth, D. Filges

Forschungszentrum Jülich, Institut für Kernphysik, Jülich, Germany

T. Ishii, M. Kuze, I. Suzuki²⁶, K. Tokushuku²⁷, S. Yamada, K. Yamauchi, Y. Yamazaki
Institute of Particle and Nuclear Studies, KEK, Tsukuba, Japan^g

S.H. Ahn, S.H. An, S.J. Hong, S.B. Lee, S.W. Nam²⁸, S.K. Park

Korea University, Seoul, Korea^h

H. Lim, I.H. Park, D. Son

Kyungpook National University, Taegu, Korea^h

F. Barreiro, J.P. Fernández, G. García, C. Glasman²⁹, J.M. Hernández³⁰, L. Labarga, J. del Peso, J. Puga, I. Redondo³¹, J. Terrón
Univer. Autónoma Madrid, Depto de Física Teórica, Madrid, Spain ⁿ

F. Corriveau, D.S. Hanna, J. Hartmann³², W.N. Murray³³, A. Ochs, S. Padhi, M. Riveline, D.G. Stairs, M. St-Laurent, M. Wing
McGill University, Dept. of Physics, Montréal, Québec, Canada ^a, ^b

T. Tsurugai
Meiji Gakuin University, Faculty of General Education, Yokohama, Japan

V. Bashkirov³⁴, B.A. Dolgoshein
Moscow Engineering Physics Institute, Moscow, Russia ^l

G.L. Bashindzhagyan, P.F. Ermolov, Yu.A. Golubkov, L.A. Khein, N.A. Korotkova, I.A. Korzhavina, V.A. Kuzmin, O.Yu. Lukina, A.S. Proskuryakov, L.M. Shcheglova³⁵, A.N. Solomin³⁵, S.A. Zotkin
Moscow State University, Institute of Nuclear Physics, Moscow, Russia ^m

C. Bokel, M. Botje, N. Brümmer, J. Engelen, E. Koffeman, P. Kooijman, A. van Sighem, H. Tiecke, N. Tuning, J.J. Velthuis, W. Verkerke, J. Vossebeld, L. Wiggers, E. de Wolf
NIKHEF and University of Amsterdam, Amsterdam, Netherlands ⁱ

D. Acosta³⁶, B. Bylsma, L.S. Durkin, J. Gilmore, C.M. Ginsburg, C.L. Kim, T.Y. Ling, P. Nylander
Ohio State University, Physics Department, Columbus, Ohio, USA ^p

H.E. Blaikley, S. Boogert, R.J. Cashmore¹⁶, A.M. Cooper-Sarkar, R.C.E. Devenish, J.K. Edmonds, J. Große-Knetter³⁷, N. Harnew, T. Matsushita, V.A. Noyes³⁸, A. Quadt¹⁶, O. Ruske, M.R. Sutton, R. Walczak, D.S. Waters
Department of Physics, University of Oxford, Oxford, U.K. ^o

A. Bertolin, R. Brugnera, R. Carlin, F. Dal Corso, S. Dondana, U. Dosselli, S. Dusini, S. Limentani, M. Morandin, M. Posocco, L. Stanco, R. Stroili, C. Voci
Dipartimento di Fisica dell' Università and INFN, Padova, Italy ^f

L. Iannotti³⁹, B.Y. Oh, J.R. Okrasinski, W.S. Toothacker, J.J. Whitmore
Pennsylvania State University, Dept. of Physics, University Park, PA, USA ^q

Y. Iga
Polytechnic University, Sagamihara, Japan ^g

G. D'Agostini, G. Marini, A. Nigro, M. Raso
Dipartimento di Fisica, Univ. 'La Sapienza' and INFN, Rome, Italy ^f

C. Cormack, J.C. Hart, N.A. McCubbin, T.P. Shah
Rutherford Appleton Laboratory, Chilton, Didcot, Oxon, U.K. ^o

D. Epperson, C. Heusch, H.F.-W. Sadrozinski, A. Seiden, R. Wichmann, D.C. Williams
University of California, Santa Cruz, CA, USA ^p

N. Pavel

Fachbereich Physik der Universität-Gesamthochschule Siegen, Germany ^c

H. Abramowicz⁴⁰, S. Dagan⁴¹, S. Kananov⁴¹, A. Kreisel, A. Levy⁴¹

Raymond and Beverly Sackler Faculty of Exact Sciences, School of Physics, Tel-Aviv University, Tel-Aviv, Israel ^e

T. Abe, T. Fusayasu, M. Inuzuka, K. Nagano, K. Umemori, T. Yamashita
Department of Physics, University of Tokyo, Tokyo, Japan ^g

R. Hamatsu, T. Hirose, K. Homma⁴², S. Kitamura⁴³, T. Nishimura
Tokyo Metropolitan University, Dept. of Physics, Tokyo, Japan ^g

M. Arneodo⁴⁴, N. Cartiglia, R. Cirio, M. Costa, M.I. Ferrero, S. Maselli, V. Monaco, C. Peroni, M. Ruspa, A. Solano, A. Staiano

Università di Torino, Dipartimento di Fisica Sperimentale and INFN, Torino, Italy ^f

M. Dardo

II Faculty of Sciences, Torino University and INFN - Alessandria, Italy ^f

D.C. Bailey, C.-P. Fagerstroem, R. Galea, T. Koop, G.M. Levman, J.F. Martin, R.S. Orr, S. Polenz, A. Sabetfakhri, D. Simmons

University of Toronto, Dept. of Physics, Toronto, Ont., Canada ^a

J.M. Butterworth, C.D. Catterall, M.E. Hayes, E.A. Heaphy, T.W. Jones, J.B. Lane, B.J. West

University College London, Physics and Astronomy Dept., London, U.K. ^o

J. Ciborowski, R. Ciesielski, G. Grzelak, R.J. Nowak, J.M. Pawlak, R. Pawlak, B. Smalska, T. Tymieniecka, A.K. Wróblewski, J.A. Zakrzewski, A.F. Żarnecki

Warsaw University, Institute of Experimental Physics, Warsaw, Poland ^j

M. Adamus, T. Gadaj

Institute for Nuclear Studies, Warsaw, Poland ^j

O. Deppe, Y. Eisenberg⁴¹, D. Hochman, U. Karshon⁴¹

Weizmann Institute, Department of Particle Physics, Rehovot, Israel ^d

W.F. Badgett, D. Chapin, R. Cross, C. Foudas, S. Mattingly, D.D. Reeder, W.H. Smith, A. Vaiciulis⁴⁵, T. Wildschek, M. Wodarczyk

University of Wisconsin, Dept. of Physics, Madison, WI, USA ^p

A. Deshpande, S. Dhawan, V.W. Hughes

Yale University, Department of Physics, New Haven, CT, USA ^p

S. Bhadra, W.R. Frisken, R. Hall-Wilton, M. Khakzad, S. Menary, W.B. Schmidke

York University, Dept. of Physics, Toronto, Ont., Canada ^a

¹ now visiting scientist at DESY
² also at IROE Florence, Italy
³ now at Univ. of Salerno and INFN Napoli, Italy
⁴ also at DESY
⁵ supported by Worldlab, Lausanne, Switzerland
⁶ now at BSG Systemplanung AG, 53757 St. Augustin
⁷ drafted to the German military service
⁸ also at University of Hamburg, Alexander von Humboldt Research Award
⁹ now at Dongshin University, Naju, Korea
¹⁰ now at NASA Goddard Space Flight Center, Greenbelt, MD 20771, USA
¹¹ supported by the Polish State Committee for Scientific Research, grant No. 2P03B14912
¹² now at Massachusetts Institute of Technology, Cambridge, MA, USA
¹³ visitor from Florida State University
¹⁴ now at Fermilab, Batavia, IL, USA
¹⁵ now at ATM, Warsaw, Poland
¹⁶ now at CERN
¹⁷ now at ESG, Munich
¹⁸ now an independent researcher in computing
¹⁹ now at University of Edinburgh, Edinburgh, U.K.
²⁰ PPARC Advanced fellow
²¹ visitor of Univ. of Crete, Greece, partially supported by DAAD, Bonn - Kz. A/98/16764
²² on leave from MSU, supported by the GIF, contract I-0444-176.07/95
²³ supported by DAAD, Bonn - Kz. A/98/12712
²⁴ supported by an EC fellowship
²⁵ PPARC Post-doctoral fellow
²⁶ now at Osaka Univ., Osaka, Japan
²⁷ also at University of Tokyo
²⁸ now at Wayne State University, Detroit
²⁹ supported by an EC fellowship number ERBFMBICT 972523
³⁰ now at HERA-B/DESY supported by an EC fellowship No.ERBFMBICT 982981
³¹ supported by the Comunidad Autonoma de Madrid
³² now at debis Systemhaus, Bonn, Germany
³³ now a self-employed consultant
³⁴ now at Loma Linda University, Loma Linda, CA, USA
³⁵ partially supported by the Foundation for German-Russian Collaboration DFG-RFBR
(grant no. 436 RUS 113/248/3 and no. 436 RUS 113/248/2)
³⁶ now at University of Florida, Gainesville, FL, USA
³⁷ supported by the Feodor Lynen Program of the Alexander von Humboldt foundation
³⁸ now with Physics World, Dirac House, Bristol, U.K.
³⁹ partly supported by Tel Aviv University
⁴⁰ an Alexander von Humboldt Fellow at University of Hamburg
⁴¹ supported by a MINERVA Fellowship
⁴² now at ICEPP, Univ. of Tokyo, Tokyo, Japan
⁴³ present address: Tokyo Metropolitan University of Health Sciences, Tokyo 116-8551,
Japan
⁴⁴ now also at Università del Piemonte Orientale, I-28100 Novara, Italy, and Alexander
von Humboldt fellow at the University of Hamburg

⁴⁵ now at University of Rochester, Rochester, NY, USA

- ^a supported by the Natural Sciences and Engineering Research Council of Canada (NSERC)
- ^b supported by the FCAR of Québec, Canada
- ^c supported by the German Federal Ministry for Education and Science, Research and Technology (BMBF), under contract numbers 057BN19P, 057FR19P, 057HH19P, 057HH29P, 057SI75I
- ^d supported by the MINERVA Gesellschaft für Forschung GmbH, the German Israeli Foundation, and by the Israel Ministry of Science
- ^e supported by the German-Israeli Foundation, the Israel Science Foundation, the U.S.-Israel Binational Science Foundation, and by the Israel Ministry of Science
- ^f supported by the Italian National Institute for Nuclear Physics (INFN)
- ^g supported by the Japanese Ministry of Education, Science and Culture (the Monbusho) and its grants for Scientific Research
- ^h supported by the Korean Ministry of Education and Korea Science and Engineering Foundation
- ⁱ supported by the Netherlands Foundation for Research on Matter (FOM)
- ^j supported by the Polish State Committee for Scientific Research, grant No. 115/E-343/SPUB/P03/154/98, 2P03B03216, 2P03B04616, 2P03B10412, 2P03B03517, and by the German Federal Ministry of Education and Science, Research and Technology (BMBF)
- ^k supported by the Polish State Committee for Scientific Research (grant No. 2P03B08614 and 2P03B06116)
- ^l partially supported by the German Federal Ministry for Education and Science, Research and Technology (BMBF)
- ^m supported by the Fund for Fundamental Research of Russian Ministry for Science and Education and by the German Federal Ministry for Education and Science, Research and Technology (BMBF)
- ⁿ supported by the Spanish Ministry of Education and Science through funds provided by CICYT
- ^o supported by the Particle Physics and Astronomy Research Council
- ^p supported by the US Department of Energy
- ^q supported by the US National Science Foundation

1 Introduction

Exclusive production of vector mesons by real and virtual photons, $\gamma p \rightarrow Vp$ and $\gamma^* p \rightarrow Vp$ ($V = \rho^0, \omega, \phi, J/\psi, \dots$), has been studied extensively, both in fixed-target experiments and at HERA [1]. For photon-proton ($\gamma^* p$) centre-of-mass energies $W \gtrsim 10$ GeV, the production of light vector mesons (ρ^0, ω, ϕ) at low photon virtuality, $Q^2 < 1$ GeV 2 , exhibits features typical of soft diffractive processes: a weak dependence on centre-of-mass energy and a differential cross section that, at low $|t|$ values, falls exponentially with $-t$, where t is the square of the four-momentum exchanged between the photon and the proton. These features are consistent with the expectations of the Vector Meson Dominance model (VMD) [2] according to which the photon is considered to fluctuate into a vector meson which then scatters elastically from the proton.

The low-energy data indicate that the amplitude for the photon/vector-meson transition is predominantly s -channel helicity conserving, i.e. the helicity of the vector meson is equal to that of the photon when the spin-quantisation axis is chosen along the direction of the meson momentum in the $\gamma^* p$ centre-of-mass system. The exchange of an object in the t -channel with $P = (-1)^J$, e.g. $J^P = 0^+, 1^-, 2^+, 3^-, \dots$ (natural parity exchange in the t channel, NPE), dominates such diffractive processes [3, 4]. However, small helicity-single-flip and helicity-double-flip contributions to the amplitude have been reported in $\pi^+ \pi^-$ photoproduction in the ρ^0 mass region at $W \lesssim 4$ GeV [5]. Helicity-single-flip amplitudes have also been observed in ρ^0 electroproduction for $1.3 < W < 2.8$ GeV and $0.3 < Q^2 < 1.4$ GeV 2 [6]. A helicity-single-flip contribution of $(14 \pm 8)\%$ was measured in ρ^0 muoproduction at $W = 17$ GeV [7].

Data from HERA have shown that when the reaction involves a large scale, such as the charm quark mass in J/ψ photoproduction [8] or high Q^2 in ρ^0 electroproduction [9, 10], the cross section rises more steeply with W and the t distribution is flatter than in the case where no such scale is present, such as ρ^0 photoproduction [11, 12, 13]. Such results can be understood in terms of models based on perturbative QCD (pQCD). In these models, the photon fluctuates into a $q\bar{q}$ pair and the interaction of the pair with the proton is mediated by the exchange of two gluons in a colour singlet state [14]. The resulting cross section is proportional to the square of the gluon density in the proton.

The cross section for the exclusive production of vector mesons from virtual photons has contributions from both transverse and longitudinal photons. These contributions are expected to have different W and Q^2 dependences [1, 15], and their extraction would provide an important test of the understanding of the production process. The angular distributions of the decay products of the vector meson, in principle, yield the separate contributions of transverse and longitudinal photons. Previous studies at HERA [9, 11, 12, 13, 16, 17, 18] assumed conservation of helicity in the s -channel amplitudes (s -channel helicity conservation, SCHC), in which case the ratio of longitudinal to transverse photon cross sections, R , is given in terms of the ratio of the number of helicity 0 (i.e. longitudinally polarised) to helicity ± 1 (i.e. transversely polarised) ρ^0 mesons produced. Sufficient data are now available to test the validity of SCHC at HERA by measuring the full set of matrix elements which completely determine the decay angular distributions. This paper reports the determination of such a set of matrix elements for exclusive ρ^0 electroproduction at HERA, $ep \rightarrow ep^0 p$ ($\rho^0 \rightarrow \pi^+ \pi^-$). Two kinematic ranges are studied,

$0.25 < Q^2 < 0.85 \text{ GeV}^2$, $20 < W < 90 \text{ GeV}$ (referred to as the “BPC” sample) and $3 < Q^2 < 30 \text{ GeV}^2$, $40 < W < 120 \text{ GeV}$ (the “DIS” sample). The two samples are those already used in the previous ZEUS paper [9], where SCHC was assumed. A similar analysis has recently been presented by the H1 Collaboration in the range $1 < Q^2 < 60 \text{ GeV}^2$ [10].

The data are used to determine R without relying on the SCHC hypothesis, to evaluate the size of the helicity-single-flip helicity-double-flip amplitudes and to test the extent to which natural parity exchange dominates in the t channel. The results are compared to recent calculations [19, 20, 21] of the amplitudes for exclusive ρ^0 meson production in the framework of pQCD models of the type described above, i.e. assuming the t -channel exchange of a gluon pair.

There are five imaginary amplitudes for ρ^0 electroproduction: two helicity-conserving amplitudes, two single-flip amplitudes, and one double-flip amplitude. The calculations indicate that, for photon virtualities exceeding the hadronic mass scale of about 1 GeV^2 , the single-flip amplitude for producing longitudinally polarised vector mesons from transverse photons is significant. This amplitude is of higher twist and vanishes in the non-relativistic limit of the ρ^0 meson wave function; in addition, it is proportional to $\sqrt{|t|}$, while the double-flip amplitude grows linearly with $|t|$. These amplitudes are small but they are rendered experimentally accessible via their interference with the dominant helicity-conserving amplitudes for longitudinal photons. Conversely, the amplitude for producing transversely polarised ρ^0 mesons from longitudinal photons is expected to be negligible [22]. There are also predictions of non-vanishing single and double-flip contributions in the non-perturbative region of small photon virtualities, $Q^2 < 1 \text{ GeV}^2$ [20, 21]. VMD-based models [23] also predict SCHC breaking on the basis of the analogy between photon-hadron and hadron-hadron interactions.

2 Experimental set-up

The data were collected at the ep collider HERA in 1995 using the ZEUS detector. In this period HERA operated at a proton energy of 820 GeV and a positron energy of 27.5 GeV , giving a total centre-of-mass energy $\sqrt{s} \simeq 300 \text{ GeV}$. A detailed description of the ZEUS detector can be found elsewhere [9, 24]. The main components used in this analysis are briefly described below.

The high-resolution uranium-scintillator calorimeter, CAL, consists of three parts: forward ¹ (FCAL), barrel (BCAL) and rear (RCAL) calorimeters. Each part is subdivided transversely into towers that are segmented longitudinally into one electromagnetic section and one (RCAL) or two (FCAL, BCAL) hadronic sections.

Charged-particle tracks are reconstructed and their momenta measured using the central tracking detector (CTD). The CTD is a cylindrical drift chamber operated in a magnetic

¹Throughout this paper the standard ZEUS right-handed coordinate system is used: the Z -axis points in the direction of the proton beam momentum (referred to as the forward direction) and the horizontal X -axis points towards the centre of HERA. The nominal interaction point is at $X = Y = Z = 0$.

field of 1.43 T produced by a superconducting solenoid. It consists of 72 cylindrical layers, organised in 9 superlayers covering the polar angular region $15^\circ < \theta < 164^\circ$.

The trajectory of positrons scattered at small angles with respect to the beam direction is determined from the beam pipe calorimeter (BPC) and the small-angle rear tracking detector (SRTD). The BPC is an electromagnetic sampling calorimeter located at $Z = -294$ cm. The SRTD is attached to the front face of the RCAL. It consists of two planes of scintillator strips, 1 cm wide and 0.5 cm thick, arranged in orthogonal orientations and read out via optical fibres and photomultiplier tubes. It covers the region of 68×68 cm² in X and Y with the exclusion of a 10×20 cm² hole at the centre for the beam pipe.

3 Kinematics and decay angular distributions

The following kinematic variables, some of which are indicated in Fig. 1, are used to describe exclusive ρ^0 production:

- The four-momenta of the incident positron (k), scattered positron (k'), incident proton (P), scattered proton (P') and virtual photon (q);
- $Q^2 = -q^2 = -(k - k')^2$, the negative four-momentum squared of the virtual photon;
- $W^2 = (q + P)^2$, the squared centre-of-mass energy of the photon-proton system;
- $y = (P \cdot q)/(P \cdot k)$, the fraction of the positron energy transferred to the proton in its rest frame;
- $M_{\pi\pi}$, the invariant mass of the two decay pions;
- $t = (P - P')^2$, the squared four-momentum transfer at the proton vertex.

The kinematic variables were reconstructed using the so-called “constrained” method [9, 25], which uses the momenta of the decay particles measured in the CTD and the polar and azimuthal angles of the scattered positron determined with the BPC (for the BPC sample) or with the CAL and the SRTD (for the DIS sample).

The exclusive electroproduction and decay of ρ^0 mesons is described, at given values of W , Q^2 , $M_{\pi\pi}$ and t , by three angles: Φ_h – the angle between the ρ^0 production plane and the positron scattering plane in the γ^*p centre-of-mass frame (see Fig. 2); θ_h and ϕ_h – the polar and azimuthal angles of the positively charged decay pion in the s -channel helicity frame, in which the spin-quantisation axis is defined as the direction opposite to the momentum of the final-state proton in the ρ^0 rest frame. In both the ρ^0 rest frame and the γ^*p centre-of-mass system, ϕ_h is the angle between the decay plane and the ρ^0 production plane. The angular distribution as a function of these three angles, $W(\cos \theta_h, \phi_h, \Phi_h)$, is parameterised by the ρ^0 spin-density matrix elements, ρ_{ik}^α , where $i, k = -1, 0, 1$ and by convention $\alpha=0,1,2,4,5,6$ for an unpolarised (or transversely polarised) charged-lepton beam [26].

The superscript denotes the decomposition of the spin-density matrix into contributions from the following photon polarisation states: unpolarised transverse photons (0); linearly polarised transverse photons (1,2); longitudinally polarised photons (4); and from the interference of the longitudinal and transverse amplitudes (5,6).

The decay angular distribution can be expressed in terms of combinations, r_{ik}^{04} and r_{ik}^α , of the density matrix elements:

$$r_{ik}^{04} = \frac{\rho_{ik}^0 + \epsilon R \rho_{ik}^4}{1 + \epsilon R}, \quad (1)$$

$$r_{ik}^\alpha = \begin{cases} \frac{\rho_{ik}^\alpha}{1 + \epsilon R}, & \alpha = 1, 2 \\ \frac{\sqrt{R} \rho_{ik}^\alpha}{1 + \epsilon R}, & \alpha = 5, 6, \end{cases} \quad (2)$$

where ϵ is the ratio of the longitudinal to transverse photon fluxes and $R = \sigma_L^{\gamma^* p} / \sigma_T^{\gamma^* p}$, with $\sigma_L^{\gamma^* p}$ and $\sigma_T^{\gamma^* p}$ the cross sections for exclusive ρ^0 production from longitudinal and transverse virtual photons, respectively. In the kinematic range of this analysis, the value of ϵ varies only between 0.98 and 1.0; hence ρ_{ik}^0 and ρ_{ik}^4 cannot be distinguished.

The hermitian nature of the spin-density matrix and the requirement of parity conservation reduces the number of independent combinations to 15, in terms of which the angular distribution can be written as

$$\begin{aligned} W(\cos \theta_h, \phi_h, \Phi_h) = & \frac{3}{4\pi} \left[\frac{1}{2}(1 - r_{00}^{04}) + \frac{1}{2}(3r_{00}^{04} - 1) \cos^2 \theta_h \right. \\ & - \sqrt{2} \operatorname{Re}\{r_{10}^{04}\} \sin 2\theta_h \cos \phi_h - r_{1-1}^{04} \sin^2 \theta_h \cos 2\phi_h \\ & - \epsilon \cos 2\Phi_h (r_{11}^1 \sin^2 \theta_h + r_{00}^1 \cos^2 \theta_h - \sqrt{2} \operatorname{Re}\{r_{10}^1\} \sin 2\theta_h \cos \phi_h \\ & \quad - r_{1-1}^1 \sin^2 \theta_h \cos 2\phi_h) \\ & - \epsilon \sin 2\Phi_h (\sqrt{2} \operatorname{Im}\{r_{10}^2\} \sin 2\theta_h \sin \phi_h + \operatorname{Im}\{r_{1-1}^2\} \sin^2 \theta_h \sin 2\phi_h) \\ & + \sqrt{2\epsilon(1 + \epsilon)} \cos \Phi_h (r_{11}^5 \sin^2 \theta_h + r_{00}^5 \cos^2 \theta_h \\ & \quad - \sqrt{2} \operatorname{Re}\{r_{10}^5\} \sin 2\theta_h \cos \phi_h - r_{1-1}^5 \sin^2 \theta_h \cos 2\phi_h) \\ & \quad \left. + \sqrt{2\epsilon(1 + \epsilon)} \sin \Phi_h (\sqrt{2} \operatorname{Im}\{r_{10}^6\} \sin 2\theta_h \sin \phi_h \right. \\ & \quad \left. \quad + \operatorname{Im}\{r_{1-1}^6\} \sin^2 \theta_h \sin 2\phi_h) \right]. \end{aligned} \quad (3)$$

The 15 coefficients r_{ik}^{04} , r_{ik}^α are related to various combinations of the helicity amplitudes $T_{\lambda_\rho \lambda_\gamma}$, where λ_ρ and λ_γ are the helicities of the ρ^0 meson and of the photon, respectively. Table 1 shows the relations between the coefficients r_{ik}^{04} , r_{ik}^α and the helicity amplitudes.

Under the SCHC assumption, the angular distribution for the decay of the ρ^0 meson depends on only two angles, θ_h and $\psi_h = \phi_h - \Phi_h$, and is characterised by three independent

parameters, r_{00}^{04} , r_{1-1}^1 and $\text{Re}\{r_{10}^5\}$:

$$\begin{aligned} W(\cos \theta_h, \psi_h) = & \frac{3}{4\pi} \left[\frac{1}{2}(1 - r_{00}^{04}) + \frac{1}{2}(3r_{00}^{04} - 1) \cos^2 \theta_h \right. \\ & \left. + \epsilon r_{1-1}^1 \sin^2 \theta_h \cos 2\psi_h - 2\sqrt{\epsilon(1 + \epsilon)} \text{Re}\{r_{10}^5\} \sin 2\theta_h \cos \psi_h \right]. \end{aligned} \quad (4)$$

The SCHC hypothesis also implies that $r_{1-1}^1 = -\text{Im}\{r_{1-1}^2\}$ and $\text{Re}\{r_{10}^5\} = -\text{Im}\{r_{10}^6\}$. In this case, the ratio R can be determined from the polar angular distribution alone:

$$R = \frac{1}{\epsilon} \frac{r_{00}^{04}}{1 - r_{00}^{04}}. \quad (5)$$

The combined assumptions of SCHC and NPE further reduce the number of independent parameters to two, since the polar and azimuthal angular distributions are then related via:

$$1 - r_{00}^{04} - 2r_{1-1}^1 = 0. \quad (6)$$

If the SCHC requirement is relaxed, then

$$R = \frac{1}{\epsilon} \frac{r_{00}^{04} - \Delta^2}{1 - (r_{00}^{04} - \Delta^2)}, \quad (7)$$

with

$$\Delta^2 = \frac{T_{01}^2 - 2T_{10}^2}{N_T + \epsilon N_L}, \quad (8)$$

where $N_L = T_{00}^2 + 2T_{10}^2$ and $N_T = T_{11}^2 + T_{1-1}^2 + T_{01}^2$. The quantity Δ can be approximated as:

$$\Delta \simeq \frac{|T_{01}|}{\sqrt{N_T + \epsilon N_L}} \simeq \frac{|T_{01}|}{\sqrt{|T_{11}|^2 + |T_{00}|^2}} \simeq \frac{r_{00}^5}{\sqrt{2r_{00}^{04}}}, \quad (9)$$

where the amplitude T_{10} (for the production of transversely polarised ρ^0 mesons from longitudinal photons) has been neglected and the amplitudes T_{00} and T_{01} are assumed to be in phase. Single and double flip amplitudes have been assumed to be small with respect to T_{00} and T_{11} .

Finally, the assumption of NPE alone leads to the sum rule:

$$1 - r_{00}^{04} + 2r_{1-1}^{04} - 2r_{11}^1 - 2r_{1-1}^1 = 0. \quad (10)$$

4 Event selection

The event selection is similar to that of the previous analysis [9]; it is summarised briefly in the following.

The online event selection required an energy deposit in the BPC or an electron candidate in the CAL, along with the detection of two tracks in the CTD.

In the offline selection the following further requirements were imposed:

- The energy of the scattered positron was required to be greater than 20 GeV if measured in the BPC and greater than 5 GeV if measured in the CAL.
- The requirement $E - p_Z > 45$ GeV was imposed, where $E - p_Z = \sum_i (E_i - p_{Z_i})$ and the summation is over the energies and longitudinal momenta of the final-state positron and pions. This cut, applied in the DIS analysis, excluded events with high energy photons radiated in the initial state.
- The Z coordinate of the interaction vertex was required to be within ± 50 cm of the nominal interaction point.
- In addition to the scattered positron, the presence of exactly two oppositely charged tracks was required, each associated with the reconstructed vertex, and each with pseudorapidity $|\eta|$ less than 1.75 and transverse momentum greater than 150 MeV; pseudorapidity is defined as $\eta = -\ln(\tan(\theta/2))$. These cuts excluded regions of low reconstruction efficiency and poor momentum resolution in the CTD.
- Events with any energy deposit larger than 300 MeV in the CAL and not associated with either the pion tracks or the positron were rejected [27, 28].

In addition, the following requirements were applied to select kinematic regions of high acceptance:

- The BPC analysis was limited to the region $0.25 < Q^2 < 0.85$ GeV 2 and $20 < W < 90$ GeV.
- The DIS analysis was restricted to the kinematic region $3 < Q^2 < 30$ GeV 2 and $40 < W < 120$ GeV.
- Only events in the $\pi^+\pi^-$ mass interval $0.6 < M_{\pi\pi} < 1.0$ GeV and with $|t| < 0.6$ GeV 2 were taken. The mass interval is slightly narrower than that used previously [9], in order to reduce the effect of the background from non-resonant $\pi^+\pi^-$ production. In the selected $M_{\pi\pi}$ range the resonant contribution is $\approx 98\%$ for the BPC sample and $\approx 100\%$ for the DIS sample.

The above selections yielded 5271 events in the BPC sample and 2510 events in the DIS sample.

5 Monte Carlo simulation

The relevant Monte Carlo generators have been described in detail previously [9]. Here their main aspects are summarised.

In the BPC analysis, a dedicated Monte Carlo generator based on the JETSET7.4 [29] package was used. The simulation of exclusive ρ^0 production was based on the VMD

model and Regge phenomenology. The effective Q^2 , W and t dependences of the cross section were parameterised to reproduce the measurements [9].

In the DIS analysis, a program [30] interfaced to HERACLES4.4 [31] was used. Again, the effective Q^2 , W and t dependences of the cross section were parameterised to reproduce the results [9].

In both cases the decay angular distributions were generated uniformly and the Monte Carlo events were then iteratively reweighted with Eq. (3) using the results of the present analysis for the 15 combinations of matrix elements r_{ik}^{04} , r_{ik}^α .

The generated events were processed through the same chain of selection and reconstruction procedures as the data, thus accounting for trigger as well as detector efficiencies and smearing effects. For both analyses, the number of simulated events after reconstruction was about a factor of seven greater than the number of reconstructed data events. Figure 3 shows the acceptances (defined as in Ref. [9]) as a function of $\cos \theta_h$, ϕ_h and Φ_h , both for the BPC and the DIS data. The different normalisations of the acceptances for the BPC and DIS samples mainly reflect the different coverage for the azimuthal angle of the scattered electron, the BPC covering only a small fraction of 2π .

6 Results

Figures 4 and 5 show the reconstructed decay angular distributions for the data (full symbols) and Monte Carlo events (solid histograms) for the BPC and for the DIS samples, respectively. The Monte Carlo simulation reproduces the measured distributions well. The dashed histograms show the same Monte Carlo events reweighted to respect SCHC. The violation of SCHC can be most clearly seen in the Φ_h distributions, particularly for the DIS sample of Fig. 5. In the following we focus on how this violation manifests itself in terms of the 15 combinations of spin-density matrix elements, r_{ik}^{04} , r_{ik}^α .

The combinations r_{ik}^{04} , r_{ik}^α were obtained by minimising the difference between the three-dimensional $(\cos \theta_h, \phi_h, \Phi_h)$ angular distributions of the data and those of the simulated events. A binned likelihood method was used, assuming a Poisson distribution for the number of events in each bin. The number of bins in $\cos \theta_h$, ϕ_h and Φ_h was $8 \times 8 \times 8$.

Table 2 summarises the results for the 15 coefficients r_{ik}^{04} , r_{ik}^α . The BPC results cover the kinematic region $0.25 < Q^2 < 0.85$ GeV 2 ($\langle Q^2 \rangle = 0.41$ GeV 2), $20 < W < 90$ GeV ($\langle W \rangle = 45$ GeV), $0.6 < M_{\pi\pi} < 1.0$ GeV and $|t| < 0.6$ GeV 2 ($\langle |t| \rangle = 0.14$ GeV 2). The DIS results cover the region $3 < Q^2 < 30$ GeV 2 ($\langle Q^2 \rangle = 6.3$ GeV 2), $40 < W < 120$ GeV ($\langle W \rangle = 73$ GeV), $0.6 < M_{\pi\pi} < 1.0$ GeV and $|t| < 0.6$ GeV 2 ($\langle |t| \rangle = 0.17$ GeV 2). Tables 3, 4 and 5 give the BPC results in bins of W , Q^2 and t . The limited statistics and poorer t resolution do not allow such fine binning for the DIS sample. Tables 6 and 7 give the full correlation matrix for the BPC and the DIS results, respectively.

Figure 6 shows the combinations of matrix elements for the BPC and the DIS data as a function of Q^2 . The coefficient r_{00}^{04} represents the probability that the ρ^0 meson be

produced in the helicity zero state, i.e. with longitudinal polarisation; it grows with Q^2 , a result qualitatively in agreement with SCHC, since the contribution of longitudinal photons increases with increasing Q^2 . Less pronounced variations with Q^2 are also observed for r_{1-1}^1 and $\text{Im}\{r_{1-1}^2\}$, which are related to r_{00}^{04} under the combined SCHC and NPE assumptions (see Sect. 3).

Figure 7 shows the coefficients r_{ik}^{04} , r_{ik}^α as functions of t for the BPC sample alone. The data suggest a growth of r_{00}^5 with $|t|$.

Figures 6, 7 and 8 compare the results to the expectations of SCHC (dashed lines) for the ten elements for which SCHC makes explicit predictions. Again deviations from SCHC are observed for both the BPC data ($\text{Re}\{r_{10}^{04}\}$, r_{1-1}^{04} , r_{11}^1 , $\text{Im}\{r_{10}^2\}$, r_{00}^5) and the DIS data (r_{00}^5). A comparison of the results with the SCHC hypothesis yields $\chi^2/ndf = 81.1/12$ for the BPC sample and $\chi^2/ndf = 79.2/12$ for the DIS sample. Figures 6 and 8 also show the recent H1 results [10], obtained in the kinematic region $1 < Q^2 < 60 \text{ GeV}^2$, $30 < W < 140 \text{ GeV}$ and $|t| < 0.5 \text{ GeV}^2$; they are in excellent agreement with the present data. The results of the model calculations [19, 20, 21] are also shown in Figs. 6 and 8.

The present results are not corrected for the contribution of non-resonant $\pi^+\pi^-$ production and its interference with resonant $\rho^0 \rightarrow \pi^+\pi^-$ production via the so-called Söding mechanism [32]. Hence, strictly speaking, they only apply to the reaction $ep \rightarrow e\pi^+\pi^-p$ with $M_{\pi\pi}$ in the quoted range. In order to assess the sensitivity of the data to changes in the selected $M_{\pi\pi}$ range – and hence changes in the relative contributions of the non-resonant and the interference terms – the events with $M_{\pi\pi} < M_\rho$ and $M_{\pi\pi} > M_\rho$ were analysed separately. For the DIS sample, where the Söding effect is small [9, 10], the results thus obtained are consistent with those found for the whole $M_{\pi\pi}$ range, suggesting that the observed breaking of SCHC is indeed a feature of the reaction $ep \rightarrow e\rho^0p$. The BPC data, however, exhibit some dependence on $M_{\pi\pi}$, as shown in Table 8. In particular, r_{00}^{04} decreases for the higher $M_{\pi\pi}$ selection, a result qualitatively consistent with expectations based on the interference between resonant and non-resonant $\pi^+\pi^-$ production [33]. The observed variations of r_{1-1}^1 and $\text{Im}\{r_{1-1}^2\}$ reflect that of r_{00}^{04} under the combined SCHC and NPE assumptions (see Sect. 3). Appreciable $M_{\pi\pi}$ dependences are also observed for r_{00}^5 , $\text{Re}\{r_{10}^5\}$ and $\text{Im}\{r_{10}^6\}$, which suggests an influence of the non-resonant $\pi^+\pi^-$ production on these combinations of matrix elements.

The results are also not corrected for the contribution from the proton-dissociative reaction, $ep \rightarrow e\rho^0N$, where N is a state of mass M_N ($M_N \lesssim 4 \text{ GeV}$) which escapes undetected in the proton beam direction. The size of this background was estimated [9] to be $(23 \pm 8)\%$ and $(24^{+9}_{-5})\%$ for the BPC and the DIS samples, respectively. The W , Q^2 , $\cos\theta_h$, ϕ_h and Φ_h distributions for the proton-dissociative events (tagged by activity in the FCAL [9]) were found to be consistent with those for the exclusive events, as expected on the basis of the factorisation of the diffractive vertices [34]. It has therefore been assumed that the proton-dissociative contribution does not affect the decay angular distributions.

Finally, any influence of radiative corrections on the angular distributions has been neglected.

7 Systematic errors

The systematic uncertainties were obtained by modifying the analysis procedures as listed below.

(a) Sensitivity to the event selection criteria:

- The $M_{\pi\pi}$ range was restricted to $0.7 < M_{\pi\pi} < 0.84$ GeV for the BPC sample and $0.65 < M_{\pi\pi} < 0.9$ GeV for the DIS sample.
- The minimum positron energy as measured in the BPC was increased to 23 GeV.
- The minimum value of $E - P_Z$ was raised to 48 GeV.
- The minimum track transverse momentum was increased from 150 MeV to 200 MeV for the BPC analysis and to 300 MeV for the DIS analysis.
- The pseudorapidity range was restricted to $|\eta| < 1.7$ for the BPC data and $|\eta| < 1.5$ for the DIS data.
- The t range was restricted to $0.05 < |t| < 0.5$ GeV 2 .

(b) Sensitivity to the Monte Carlo simulation:

- The W distribution was reweighted by a factor W^k , with k varying between -0.1 and 0.1 .
- The Q^2 distribution was reweighted by a factor $1/(1+Q^2/M_\rho^2)^k$, where k varies between -0.2 and 0.2 and M_ρ is the ρ^0 meson mass.
- The t slope was varied by ± 1 GeV $^{-2}$ for the BPC data and by ± 0.5 GeV $^{-2}$ for the DIS data.

(c) Sensitivity to the fitting procedure: the method of moments was used instead of the maximum likelihood method. Moments of the observed three-dimensional distribution in the angles ($\cos \theta_h$, ϕ_h and Φ_h) were calculated, i.e. the distribution was projected on appropriate functions of $\cos \theta_h$, ϕ_h and Φ_h . The same moments were evaluated for the reconstructed angular distribution from the Monte Carlo simulation and the difference between the moments in the data and those in the Monte Carlo was minimised by adjusting the values of the coefficients r_{ik}^{04} , r_{ik}^α used in the simulation. This method is a variation of that presented in Appendix C of Ref. [26].

(d) Sensitivity to the binning: the standard number of bins in $\cos \theta_h$, ϕ_h and Φ_h , $8 \times 8 \times 8$, was changed to $6 \times 8 \times 8$ bins and, in the BPC case, also to $10 \times 10 \times 10$.

The dominant effects come from the sensitivity to the binning, the modification of the $M_{\pi\pi}$ range and the fitting method (maximum likelihood vs method of moments). As an example, for r_{00}^5 , the systematic uncertainty due to the binning is 26% (14%), and that due to the $M_{\pi\pi}$ range is 15% (11%) for the BPC (DIS) analysis.

8 Discussion

In this section the r_{ik}^{04} , r_{ik}^α combinations which exhibit a deviation from SCHC are individually examined. The implications of the measured violation of SCHC for $R = \sigma_L^{\gamma^* p} / \sigma_T^{\gamma^* p}$ are also discussed, as is the extent to which NPE dominates the present data.

Deviations from the null values expected in the case of SCHC are observed for $\text{Re}\{r_{10}^{04}\}$, r_{1-1}^{04} , r_{11}^1 , $\text{Im}\{r_{10}^2\}$ and r_{00}^5 :

1. $\text{Re}\{r_{10}^{04}\} = 0.034 \pm 0.006$ (stat.) ± 0.009 (syst.) for the BPC sample. The DIS sample gives $\text{Re}\{r_{10}^{04}\} = 0.013 \pm 0.010$ (stat.) ± 0.022 (syst.), which is consistent with the BPC result but does not significantly deviate from zero. The H1 DIS result, $\text{Re}\{r_{10}^{04}\} = 0.011 \pm 0.012$ (stat.) $^{+0.007}_{-0.001}$ (syst.), is consistent with zero [10].

Non-zero values of $\text{Re}\{r_{10}^{04}\}$ have also been observed in low-energy photoproduction [5], as well as in electroproduction [6] and muoproduction [7] experiments. Reference [6] quotes values ranging from 0.01 to 0.16 for $0 \lesssim Q^2 \lesssim 1$ GeV 2 and $1.7 < W < 2.8$ GeV. At higher energy, $12.5 < W < 16$ GeV, and for $Q^2 < 3$ GeV 2 , the CHIO Collaboration found $\text{Re}\{r_{10}^{04}\} = 0.07 \pm 0.03$ [7].

This coefficient is sensitive (cf. Table 1) to the interference of helicity-conserving and helicity-single-flip amplitudes, as well as to the interference of helicity-single-flip and helicity-double-flip amplitudes. Both single-flip amplitudes are involved here, i.e. that for the production of longitudinally polarised ρ^0 mesons from transverse photons and that for the production of transversely polarised mesons from longitudinal photons.

The data are consistent with the pQCD predictions of [20, 21] at low Q^2 . Some disagreement with the predictions of [19, 21] is visible at high Q^2 .

2. $r_{1-1}^{04} = -0.040 \pm 0.009$ (stat.) ± 0.019 (syst.) for the BPC sample. No deviation from zero is observed for the DIS sample, $r_{1-1}^{04} = 0.000 \pm 0.011$ (stat.) ± 0.008 (syst.). The H1 DIS result, $r_{1-1}^{04} = -0.010 \pm 0.013$ (stat.) $^{+0.004}_{-0.003}$ (syst.), is consistent with zero [10].

Negative values for r_{1-1}^{04} , consistent with the BPC result, though only marginally different from zero, were also measured in the range $1.7 < W < 2$ GeV, $Q^2 < 1$ GeV 2 [6]. A value of $r_{1-1}^{04} = -0.07 \pm 0.03$ was reported for $12.5 < W < 16$ GeV [7]. Negative values of ρ_{1-1}^0 were measured in photoproduction [5].

This term is proportional to the square of the helicity-single-flip amplitude for the production of transversely polarised ρ^0 mesons from longitudinal photons, T_{10} , and is also sensitive to the interference of helicity-conserving and helicity-double-flip amplitudes.

For this combination of matrix elements, as for $\text{Re}\{r_{10}^{04}\}$ discussed above, the relative contribution from longitudinal photons is an order of magnitude larger for the DIS sample than for the BPC sample, owing to the Q^2 dependence of R (see Eq. 1).

The pQCD based models [19, 20, 21] reproduce the DIS data for r_{1-1}^{04} . At low Q^2 some disagreement between the model [21] and the data is observed.

3. $r_{11}^1 = -0.039 \pm 0.009$ (stat.) ± 0.021 (syst.) for the BPC sample. Here again, no significant effect is visible in the DIS data, $r_{11}^1 = -0.006 \pm 0.012$ (stat.) ± 0.026 (syst.). No evidence for a deviation from zero of r_{11}^1 was found by the fixed-target experiments or by H1; the latter measured $r_{11}^1 = -0.002 \pm 0.034$ (stat.) ± 0.006 (syst.) in DIS [10].

This coefficient is sensitive to the interference between the helicity-conserving and the helicity-double-flip amplitudes.

Here also the models [19, 20, 21] reproduce the DIS data. At low Q^2 disagreements similar to those observed for r_{1-1}^{04} between the model [21] and the data are visible.

4. $\text{Im}\{r_{10}^2\} = 0.039 \pm 0.008$ (stat.) ± 0.012 (syst.) (BPC). The DIS result, $\text{Im}\{r_{10}^2\} = 0.008 \pm 0.014$ (stat.) ± 0.031 (syst.), is consistent with zero, although also consistent with the BPC result. The H1 DIS result, $\text{Im}\{r_{10}^2\} = 0.023 \pm 0.016$ (stat.) $^{+0.010}_{-0.009}$ (syst.), is also consistent with zero [10]. No significant deviation of $\text{Im}\{r_{10}^2\}$ from zero was found in the earlier experiments.

This coefficient is sensitive to the interference of helicity-conserving and helicity-single-flip amplitudes as well as to the interference of single-flip and double-flip amplitudes. The single-flip amplitude involved is that corresponding to the production of longitudinally polarised ρ^0 mesons from transverse photons.

The pQCD based models [19, 20, 21] give a satisfactory description of the data.

5. $r_{00}^5 = 0.051 \pm 0.010$ (stat.) ± 0.018 (syst.) (BPC) and $r_{00}^5 = 0.095 \pm 0.019$ (stat.) ± 0.024 (syst.) (DIS). The H1 experiment found $r_{00}^5 = 0.093 \pm 0.024$ (stat.) $^{+0.019}_{-0.010}$ (syst.) in DIS [10], in good agreement with the present ZEUS DIS result. None of the fixed-target experiments measured significant deviations from zero for r_{00}^5 .

This coefficient is proportional to the interference between the helicity-non-flip amplitude for longitudinal photons T_{00} and the helicity-single-flip amplitude T_{01} for the production of longitudinally polarised ρ^0 mesons from transverse photons. The BPC data suggest that r_{00}^5 increases with increasing $|t|$.

The deviation of r_{00}^5 from zero is directly related to the failure of SCHC to describe the Φ_h distribution (cf. Figs. 4 and 5), as is apparent by integrating Eq. (3) over $\cos \theta_h$ and ϕ_h :

$$W(\Phi_h) \propto [1 - \epsilon \cos 2\Phi_h(2r_{11}^1 + r_{00}^1) + \sqrt{2\epsilon(1+\epsilon)} \cos \Phi_h(2r_{11}^5 + r_{00}^5)]. \quad (11)$$

The results for r_{00}^5 are consistent with the predictions of refs. [19, 20, 21], with the possible exception of model [21], which at large Q^2 is somewhat higher than the data.

The SCHC-breaking effects observed are not large. This can be seen, for instance, from the fact that the SCHC-based relations $r_{1-1}^1 = -\text{Im}\{r_{1-1}^2\}$, $\text{Re}\{r_{10}^5\} = -\text{Im}\{r_{10}^6\}$ are

satisfied within errors:

$$\begin{aligned} r_{1-1}^1 + \text{Im}\{r_{1-1}^2\} &= 0.003 \pm 0.016 \text{ (stat.)} \pm 0.030 \text{ (syst.) (BPC),} \\ r_{1-1}^1 + \text{Im}\{r_{1-1}^2\} &= -0.037 \pm 0.028 \text{ (stat.)} \pm 0.038 \text{ (syst.) (DIS),} \end{aligned}$$

$$\begin{aligned} \text{Re}\{r_{10}^5\} + \text{Im}\{r_{10}^6\} &= 0.001 \pm 0.005 \text{ (stat.)} \pm 0.013 \text{ (syst.) (BPC),} \\ \text{Re}\{r_{10}^5\} + \text{Im}\{r_{10}^6\} &= 0.006 \pm 0.012 \text{ (stat.)} \pm 0.011 \text{ (syst.) (DIS).} \end{aligned}$$

The relation $1 - r_{00}^{04} - 2r_{1-1}^1 = 0$ (which requires NPE in addition to SCHC) is also satisfied, but only within approximately 1.6 standard deviations (summing statistical and systematic uncertainties in quadrature) for the DIS data:

$$\begin{aligned} 1 - r_{00}^{04} - 2r_{1-1}^1 &= 0.060 \pm 0.021 \text{ (stat.)} \pm 0.047 \text{ (syst.) (BPC),} \\ 1 - r_{00}^{04} - 2r_{1-1}^1 &= 0.079 \pm 0.032 \text{ (stat.)} \pm 0.036 \text{ (syst.) (DIS).} \end{aligned}$$

The ratio of the ρ^0 electroproduction cross section for longitudinal photons to that for transverse photons, R , was also determined under a much weaker set of assumptions than SCHC (Eqs. (7)-(9)). The BPC data give $R = 0.368^{+0.021}_{-0.020}$ (stat.) $^{+0.024}_{-0.023}$ (syst.), to be compared with the SCHC-based value $R = 0.377 \pm 0.021$ (stat.) ± 0.021 (syst.). The DIS data yield $R = 2.58^{+0.16}_{-0.15}$ (stat.) $^{+0.24}_{-0.21}$ (syst.) while the SCHC-based value is $R = 2.66^{+0.17}_{-0.15}$ (stat.) $^{+0.24}_{-0.21}$ (syst.). The new results differ from the value derived from the SCHC hypothesis by less than 3% when averaged over either the BPC or DIS data samples. It can therefore be concluded that the results for R presented in Ref.[9] are not significantly influenced by the SCHC assumption used in obtaining them.

The size of the SCHC-breaking effects can also be quantified by evaluating the ratios of the helicity-single-flip and helicity-double-flip amplitudes to the helicity-conserving amplitudes:

- The ratio of T_{01} (for the production of longitudinally polarised ρ^0 mesons from transverse photons) to the helicity-conserving amplitudes can be estimated as (cf. Eq. (9))

$$\tau_{01} = \frac{|T_{01}|}{\sqrt{|T_{00}|^2 + |T_{11}|^2}} \simeq \frac{r_{00}^5}{\sqrt{2r_{00}^{04}}}; \quad (12)$$

this relation holds if T_{00} and T_{01} have the same phase and if the term $T_{01}^2/(N_T + \epsilon N_L)$ is negligible. Equation (12) gives $\tau_{01} = (6.9 \pm 1.3 \text{ (stat.)} \pm 2.4 \text{ (syst.)})\%$ for the BPC data and $\tau_{01} = (7.9 \pm 1.6 \text{ (stat.)} \pm 2.0 \text{ (syst.)})\%$ for the DIS data. The H1 result for this quantity is $(8 \pm 3)\%$ [10].

- Likewise, the ratio

$$\tau_{10} = \frac{|T_{10}|}{\sqrt{|T_{00}|^2 + |T_{11}|^2}} \simeq \frac{|\text{Re}\{r_{10}^{04}\} + \text{Re}\{r_{10}^1\}|}{\sqrt{r_{00}^{04}}} \quad (13)$$

can be evaluated, where T_{10} is the amplitude for the production of transversely polarised ρ^0 mesons from longitudinal photons. Equation (13) is exact if NPE holds and T_{00} and T_{10} have the same phase. The value $\tau_{10} = (2.9 \pm 1.4 \text{ (stat.)} \pm 3.0 \text{ (syst.)})\%$ is found for the BPC sample and $\tau_{10} = (2.7 \pm 1.9 \text{ (stat.)} \pm 3.1 \text{ (syst.)})\%$ for the DIS data. These results are consistent with the expectation of a severe suppression of the production of transversely polarised ρ^0 mesons from longitudinal photons [22].

- The size of the helicity-double-flip amplitude T_{1-1} can be derived assuming NPE and the same phase for T_{1-1} and T_{11} :

$$\tau_{1-1} = \frac{|T_{1-1}|}{\sqrt{|T_{00}|^2 + |T_{11}|^2}} \simeq \frac{|r_{11}^1|}{\sqrt{2r_{1-1}^1}}, \quad (14)$$

which gives $\tau_{1-1} = (4.8 \pm 1.1 \text{ (stat.)} \pm 2.6 \text{ (syst.)})\%$ in the BPC analysis and $\tau_{1-1} = (1.4 \pm 2.7 \text{ (stat.)} \pm 5.9 \text{ (syst.)})\%$ for the DIS sample.

Finally, the data can be used to verify the validity of the NPE hypothesis. The left-hand-side of Eq. (10) is $0.058 \pm 0.027 \text{ (stat.)} \pm 0.074 \text{ (syst.)}$ for the BPC sample and $0.091 \pm 0.016 \text{ (stat.)} \pm 0.065 \text{ (syst.)}$ for the DIS sample. Both results are consistent with the NPE expectation of zero.

9 Summary and conclusions

Exclusive electroproduction of ρ^0 mesons has been measured at HERA in two Q^2 ranges, $0.25 < Q^2 < 0.85 \text{ GeV}^2$ and $3 < Q^2 < 30 \text{ GeV}^2$, and the angular distributions of the decay pions have been studied. The low- Q^2 data span the range $20 < W < 90 \text{ GeV}$; the high- Q^2 data cover the $40 < W < 120 \text{ GeV}$ interval. Both samples extend up to $|t| = 0.6 \text{ GeV}^2$. The available statistics enable a determination of the 15 combinations of spin-density matrix elements, r_{ik}^{04} and r_{ik}^α , and allow a check of the extent to which s -channel helicity conservation holds at HERA energies for this process. An overall comparison of the data with the SCHC hypothesis leads to a very poor χ^2 , $\chi^2/ndf = 81.1/12$, for the BPC sample and $\chi^2/ndf = 79.2/12$ for the DIS sample. The deviation from SCHC is most evident in the Φ_h distribution.

In the low- Q^2 sample, five of the r_{ik}^{04} and r_{ik}^α combinations deviate from the null value expected if SCHC is assumed. The combination r_{00}^5 is measured to be $r_{00}^5 = 0.051 \pm 0.010 \text{ (stat.)} \pm 0.018 \text{ (syst.)}$, which indicates the production of longitudinally polarised (i.e. helicity zero) ρ^0 mesons from transverse photons. In addition, $\text{Re}\{r_{10}^{04}\} = 0.034 \pm$

0.006 (stat.) ± 0.009 (syst.), $r_{1-1}^{04} = -0.040 \pm 0.009$ (stat.) ± 0.019 (syst.), $r_{11}^1 = -0.039 \pm 0.009$ (stat.) ± 0.021 (syst.) and $\text{Im}\{r_{10}^2\} = 0.039 \pm 0.008$ (stat.) ± 0.012 (syst.). The measured values for $\text{Re}\{r_{10}^{04}\}$ and r_{1-1}^{04} are consistent with the results of earlier fixed-target experiments. Some variation of these results with $M_{\pi\pi}$ is observed, possibly indicating a contribution from non-resonant $\pi^+\pi^-$ production and its interference with resonant ρ^0 production.

In the high- Q^2 sample, the only coefficient significantly different from the SCHC expectation is r_{00}^5 , for which the value $r_{00}^5 = 0.095 \pm 0.019$ (stat.) ± 0.024 (syst.) is measured. This value of r_{00}^5 is consistent with the predictions of the pQCD based models [19, 20, 21]. The results for all coefficients r_{ik}^{04} and r_{ik}^a at large Q^2 are in good agreement with those found by H1 [10].

The ratio R of the cross sections for ρ^0 production from longitudinal and transverse photons was also determined without assuming SCHC. The results thus found differ from those derived from the SCHC hypothesis by less than 3% when averaged over either the BPC or DIS data samples. The results for R presented in Ref.[9] are thus not significantly influenced by the SCHC assumption used in obtaining them.

Finally, the data support the hypothesis of natural parity exchange in ρ^0 electroproduction.

In conclusion, a small breaking of SCHC, less than 10% in the amplitudes, is a characteristic feature of exclusive ρ^0 meson production also at the large values of W accessible at HERA. In the high- Q^2 region, the effect is quantitatively reproduced by perturbative QCD calculations.

Acknowledgements

We thank the DESY Directorate for their strong support and encouragement, and the HERA machine group for their diligent efforts. We are grateful for the support of the DESY computing and network services. The design, construction and installation of the ZEUS detector have been made possible by the ingenuity and effort of many people from DESY and home institutes who are not listed as authors. It is also a pleasure to thank I. Akushevich, M. Diehl, D.Yu. Ivanov, N.N. Nikolaev, I. Royen, M.G. Ryskin, Yu.M. Shabelski and B.G. Zakharov for many useful discussions. We are grateful to I. Akushevich and I. Royen for calculating the predictions of their models for the kinematic range covered by our data.

References

- [1] J.A. Crittenden, “Exclusive Production of Neutral Vector Mesons at the Electron-Proton Collider HERA”, Springer Tracts in Modern Physics, Volume 140, Springer, Berlin and Heidelberg (1997), and references therein.

- [2] J.J. Sakurai, “Currents and Mesons”, University of Chicago Press, Chicago (1969); H. Fraas and D. Schildknecht, Nucl. Phys. B14 (1969) 543.
- [3] T.H. Bauer et al., Rev. Mod. Phys. 50 (1978) 261, Erratum ibid. 51 (1979) 407, and references therein.
- [4] P.D.B. Collins, “An Introduction to Regge Theory and High Energy Physics”, Cambridge University Press, Cambridge (1977).
- [5] J. Ballam et al., Phys. Rev. D7 (1973) 3150.
- [6] P. Joos et al., Nucl. Phys. B113 (1976) 53.
- [7] CHIO Collab., W.D. Shambroom et al., Phys. Rev. D26 (1982) 1.
- [8] H1 Collab., S. Aid et al., Nucl. Phys. B472 (1996) 3;
ZEUS Collab., J. Breitweg et al., Z. Phys. C75 (1997) 215.
- [9] ZEUS Collab., J. Breitweg et al., Eur. Phys. J. C6 (1999) 603.
- [10] H1 Collab., C. Adloff et al., DESY Report DESY 99-010, hep-ex/9902019 (1999), to appear in Eur. Phys. J. C.
- [11] ZEUS Collab., M. Derrick et al., Z. Phys. C69 (1995) 39.
- [12] H1 Collab., S. Aid et al., Nucl. Phys. B463 (1996) 3.
- [13] ZEUS Collab., J. Breitweg et al., Eur. Phys. J. C2 (1998) 247.
- [14] H. Abramowicz et al., in *Proceedings of the Workshop on Future Physics at HERA, Volume II*, edited by G. Ingelman, A. De Roeck and R. Klanner (DESY, Hamburg, Germany, 1996), p. 635, and references therein;
W. Koepf et al., ibid., p. 674, and references therein.
- [15] J.C. Collins, L.L. Frankfurt and M. Strikman, Phys. Rev. D56 (1997) 2982.
- [16] ZEUS Collab., M. Derrick et al., Phys. Lett. B356 (1995) 601.
- [17] H1 Collab., S. Aid et al., Nucl. Phys. B468 (1996) 3.
- [18] H1 Collab., C. Adloff et al., Z. Phys. C75 (1997) 607.
- [19] D. Yu. Ivanov and R. Kirschner, Phys. Rev. D58 (1998) 114026.
- [20] E.V. Kuraev, N.N. Nikolaev and B.G. Zakharov, JETP Lett. 68 (1998) 696 and Pisma Zh. Eksp. Teor. Fiz. 68 (1998) 667;
N.N. Nikolaev, Proceedings of the DIS99 workshop, April 19-23, 1999, Zeuthen, Germany, Eds. J. Blümlein and T. Riemann, to appear in Nucl. Phys. B (Proc. Suppl.);
I. Akushevich, I. Ivanov, N.N. Nikolaev and A. Pronyaev, private communication.

- [21] I. Royen, Proceedings of the DIS99 workshop, April 19-23, 1999, Zeuthen, Germany, Eds. J. Blümlein and T. Riemann, to appear in Nucl. Phys. B (Proc. Suppl.) and Liège University preprint ULG-PNT-99-1-IR; I. Royen, private communication.
- [22] M. Diehl et al., Phys. Rev. D59 (1999) 34023.
- [23] D. Schildknecht, G. A. Schuler and B. Surrow, Phys. Lett. B449 (1999) 328.
- [24] ZEUS Collab., “The ZEUS Detector Status report”, DESY (1993).
- [25] ZEUS Collab., M. Derrick et al., Phys. Lett. B356 (1995) 601.
- [26] K. Schilling and G. Wolf, Nucl. Phys. B61 (1973) 381.
- [27] H. Beier, Ph.D. thesis, Hamburg University (1997), DESY Internal Report DESY F35D-97-06.
- [28] T. Monteiro, Ph.D. thesis, Hamburg University (1998), DESY Internal Report DESY-THESIS-1998-027.
- [29] T. Sjöstrand, Comp. Phys. Commun. 39 (1986) 347; T. Sjöstrand and M. Bengtsson, Comp. Phys. Commun. 43 (1987) 367.
- [30] K. Muchorowski, Ph.D. thesis, Warsaw University (1998).
- [31] A. Kwiatkowski, H. Spiesberger and H.-J. Moehring, in *Proceedings of the Workshop on Physics at HERA, Volume III*, edited by W. Buchmüller and G. Ingelman (DESY, Hamburg, Germany, 1991), p. 1294.
- [32] P. Söding, Phys. Lett. 19 (1966) 702.
- [33] M.G. Ryskin and Yu.M. Shabelski, Phys. At. Nucl. 61 (1988) 81.
- [34] G. Alberi and G. Goggi, Phys. Rep. 74 (1981) 1; K. Goulian, Phys. Rep. 101 (1983) 169; N.P. Zotov and V.A. Tsarev, Sov. Phys. Uspekhi 31 (1988) 119; G. Giacomelli, Int. J. Mod. Phys. A5 (1990) 223.

$$r_{00}^{04} = \frac{\epsilon T_{00}^2}{N_T + \epsilon N_L} + \frac{T_{01}^2}{N_T + \epsilon N_L}$$

$$\text{Re}\{r_{10}^{04}\} = \frac{1}{2} \frac{\text{Re}\{T_{11}T_{01}^*\}}{N_T + \epsilon N_L} + \frac{\epsilon \text{Re}\{T_{10}T_{00}^*\}}{N_T + \epsilon N_L} + \frac{1}{2} \frac{\text{Re}\{T_{1-1}T_{0-1}^*\}}{N_T + \epsilon N_L}$$

$$r_{1-1}^{04} = -\frac{\epsilon T_{10}^2}{N_T + \epsilon N_L} + \frac{\text{Re}\{T_{11}T_{1-1}^*\}}{N_T + \epsilon N_L}$$

$$r_{11}^1 = \frac{\text{Re}\{T_{1-1}T_{11}^*\}}{N_T + \epsilon N_L}$$

$$r_{00}^1 = -\frac{T_{01}^2}{N_T + \epsilon N_L}$$

$$\text{Re}\{r_{10}^1\} = \frac{1}{2} \frac{\text{Re}\{T_{11}T_{0-1}^*\}}{N_T + \epsilon N_L} + \frac{1}{2} \frac{\text{Re}\{T_{1-1}T_{01}^*\}}{N_T + \epsilon N_L}$$

$$r_{1-1}^1 = \frac{1}{2} \frac{T_{11}^2}{N_T + \epsilon N_L} + \frac{1}{2} \frac{T_{1-1}^2}{N_T + \epsilon N_L}$$

$$\text{Im}\{r_{10}^2\} = -\frac{1}{2} \frac{\text{Re}\{T_{11}T_{0-1}^*\}}{N_T + \epsilon N_L} + \frac{1}{2} \frac{\text{Re}\{T_{1-1}T_{01}^*\}}{N_T + \epsilon N_L}$$

$$\text{Im}\{r_{1-1}^2\} = -\frac{1}{2} \frac{T_{11}^2}{N_T + \epsilon N_L} + \frac{1}{2} \frac{T_{1-1}^2}{N_T + \epsilon N_L}$$

$$r_{11}^5 = \frac{1}{\sqrt{2}} \frac{\text{Re}\{T_{10}T_{11}^*\}}{N_T + \epsilon N_L} - \frac{1}{\sqrt{2}} \frac{\text{Re}\{T_{10}T_{1-1}^*\}}{N_T + \epsilon N_L}$$

$$r_{00}^5 = \frac{\sqrt{2} \text{Re}\{T_{00}T_{01}^*\}}{N_T + \epsilon N_L}$$

$$\text{Re}\{r_{10}^5\} = \frac{1}{2\sqrt{2}} \frac{\text{Re}\{T_{11}T_{00}^*\}}{N_T + \epsilon N_L} + \frac{1}{\sqrt{2}} \frac{\text{Re}\{T_{10}T_{01}^*\}}{N_T + \epsilon N_L} - \frac{1}{2\sqrt{2}} \frac{\text{Re}\{T_{1-1}T_{00}^*\}}{N_T + \epsilon N_L}$$

$$r_{1-1}^5 = \frac{1}{\sqrt{2}} \frac{\text{Re}\{T_{11}T_{-10}^*\}}{N_T + \epsilon N_L} + \frac{1}{\sqrt{2}} \frac{\text{Re}\{T_{10}T_{-11}^*\}}{N_T + \epsilon N_L}$$

$$\text{Im}\{r_{10}^6\} = -\frac{1}{2\sqrt{2}} \frac{\text{Re}\{T_{11}T_{00}^*\}}{N_T + \epsilon N_L} - \frac{1}{2\sqrt{2}} \frac{\text{Re}\{T_{1-1}T_{00}^*\}}{N_T + \epsilon N_L}$$

$$\text{Im}\{r_{1-1}^6\} = -\frac{1}{\sqrt{2}} \frac{\text{Re}\{T_{-10}T_{11}^*\}}{N_T + \epsilon N_L} + \frac{1}{\sqrt{2}} \frac{\text{Re}\{T_{10}T_{-11}^*\}}{N_T + \epsilon N_L}$$

$$\text{where } N_L = T_{00}^2 + 2T_{10}^2 \quad N_T = T_{11}^2 + T_{1-1}^2 + T_{01}^2$$

Table 1: The 15 combinations of spin-density matrix elements r_{ik}^{04} , r_{ik}^α , expressed in terms of the helicity amplitudes; natural parity exchange in the t channel is assumed for r_{1-1}^{04} , r_{00}^1 , r_{1-1}^1 , $\text{Im}\{r_{1-1}^2\}$, $\text{Re}\{r_{10}^5\}$, $\text{Im}\{r_{10}^6\}$.

	ZEUS 1995 (BPC)	ZEUS 1995 (DIS)
r_{00}^{04}	$0.272 \pm 0.011 \pm 0.011$	$0.725 \pm 0.012 \pm 0.017$
$\text{Re}\{r_{10}^{04}\}$	$0.034 \pm 0.006 \pm 0.009$	$0.013 \pm 0.010 \pm 0.022$
r_{1-1}^{04}	$-0.040 \pm 0.009 \pm 0.019$	$0.000 \pm 0.011 \pm 0.008$
r_{11}^1	$-0.039 \pm 0.009 \pm 0.021$	$-0.006 \pm 0.012 \pm 0.026$
r_{00}^1	$0.004 \pm 0.015 \pm 0.038$	$-0.013 \pm 0.041 \pm 0.076$
$\text{Re}\{r_{10}^1\}$	$-0.019 \pm 0.008 \pm 0.013$	$-0.036 \pm 0.015 \pm 0.015$
r_{1-1}^1	$0.334 \pm 0.011 \pm 0.023$	$0.098 \pm 0.016 \pm 0.016$
$\text{Im}\{r_{10}^2\}$	$0.039 \pm 0.008 \pm 0.012$	$0.008 \pm 0.014 \pm 0.031$
$\text{Im}\{r_{1-1}^2\}$	$-0.331 \pm 0.011 \pm 0.020$	$-0.135 \pm 0.017 \pm 0.035$
r_{11}^5	$0.008 \pm 0.004 \pm 0.012$	$0.018 \pm 0.005 \pm 0.012$
r_{00}^5	$0.051 \pm 0.010 \pm 0.018$	$0.095 \pm 0.019 \pm 0.024$
$\text{Re}\{r_{10}^5\}$	$0.142 \pm 0.004 \pm 0.012$	$0.142 \pm 0.007 \pm 0.008$
r_{1-1}^5	$-0.010 \pm 0.006 \pm 0.008$	$-0.003 \pm 0.008 \pm 0.005$
$\text{Im}\{r_{10}^6\}$	$-0.141 \pm 0.003 \pm 0.005$	$-0.136 \pm 0.007 \pm 0.008$
$\text{Im}\{r_{1-1}^6\}$	$0.014 \pm 0.006 \pm 0.007$	$0.009 \pm 0.008 \pm 0.018$

Table 2: The 15 combinations of spin-density matrix elements r_{ik}^{04} , r_{ik}^α , as obtained from the BPC and DIS data sets. Statistical and systematic uncertainties are given separately. The BPC data cover the kinematic range $0.25 < Q^2 < 0.85 \text{ GeV}^2$ ($\langle Q^2 \rangle = 0.41 \text{ GeV}^2$), $20 < W < 90 \text{ GeV}$ ($\langle W \rangle = 45 \text{ GeV}$), $0.6 < M_{\pi\pi} < 1.0 \text{ GeV}$ and $|t| < 0.6 \text{ GeV}^2$ ($\langle |t| \rangle = 0.14 \text{ GeV}^2$). The DIS data cover the kinematic range $3 < Q^2 < 30 \text{ GeV}^2$ ($\langle Q^2 \rangle = 6.3 \text{ GeV}^2$), $40 < W < 120 \text{ GeV}$ ($\langle W \rangle = 73 \text{ GeV}$), $0.6 < M_{\pi\pi} < 1.0 \text{ GeV}$ and $|t| < 0.6 \text{ GeV}^2$ ($\langle |t| \rangle = 0.17 \text{ GeV}^2$).

ZEUS 1995 (BPC)		
	$20 < W < 45$ GeV	$45 < W < 90$ GeV
r_{00}^{04}	$0.293 \pm 0.014 \pm 0.016$	$0.257 \pm 0.017 \pm 0.021$
$\text{Re}\{r_{10}^{04}\}$	$0.034 \pm 0.009 \pm 0.008$	$0.027 \pm 0.010 \pm 0.005$
r_{1-1}^{04}	$-0.032 \pm 0.011 \pm 0.009$	$-0.056 \pm 0.013 \pm 0.020$
r_{11}^1	$-0.040 \pm 0.012 \pm 0.006$	$-0.038 \pm 0.015 \pm 0.007$
r_{00}^1	$0.004 \pm 0.021 \pm 0.030$	$0.003 \pm 0.025 \pm 0.051$
$\text{Re}\{r_{10}^1\}$	$-0.024 \pm 0.011 \pm 0.016$	$-0.012 \pm 0.013 \pm 0.005$
r_{1-1}^1	$0.328 \pm 0.015 \pm 0.014$	$0.345 \pm 0.018 \pm 0.018$
$\text{Im}\{r_{10}^2\}$	$0.037 \pm 0.010 \pm 0.013$	$0.038 \pm 0.012 \pm 0.006$
$\text{Im}\{r_{1-1}^2\}$	$-0.313 \pm 0.015 \pm 0.023$	$-0.348 \pm 0.018 \pm 0.022$
r_{11}^5	$0.015 \pm 0.006 \pm 0.008$	$0.004 \pm 0.007 \pm 0.010$
r_{00}^5	$0.039 \pm 0.013 \pm 0.016$	$0.050 \pm 0.016 \pm 0.007$
$\text{Re}\{r_{10}^5\}$	$0.143 \pm 0.005 \pm 0.008$	$0.142 \pm 0.006 \pm 0.013$
r_{1-1}^5	$-0.013 \pm 0.008 \pm 0.007$	$-0.008 \pm 0.009 \pm 0.010$
$\text{Im}\{r_{10}^6\}$	$-0.150 \pm 0.004 \pm 0.004$	$-0.131 \pm 0.006 \pm 0.007$
$\text{Im}\{r_{1-1}^6\}$	$0.011 \pm 0.007 \pm 0.004$	$0.022 \pm 0.009 \pm 0.007$

Table 3: The 15 combinations of spin-density matrix elements r_{ik}^{04} , r_{ik}^α , as obtained from the BPC data in two W intervals. Statistical and systematic uncertainties are given separately. The data cover the kinematic range $0.25 < Q^2 < 0.85$ GeV 2 , $20 < W < 90$ GeV, $0.6 < M_{\pi\pi} < 1.0$ GeV and $|t| < 0.6$ GeV 2 . The average W values for the two intervals are $\langle W \rangle = 31$ GeV and $\langle W \rangle = 61$ GeV, respectively.

ZEUS 1995 (BPC)		
	$0.25 < Q^2 < 0.4 \text{ GeV}^2$	$0.4 < Q^2 < 0.85 \text{ GeV}^2$
r_{00}^{04}	$0.228 \pm 0.016 \pm 0.022$	$0.324 \pm 0.015 \pm 0.012$
$\text{Re}\{r_{10}^{04}\}$	$0.025 \pm 0.009 \pm 0.004$	$0.040 \pm 0.010 \pm 0.009$
r_{1-1}^{04}	$-0.053 \pm 0.012 \pm 0.003$	$-0.028 \pm 0.012 \pm 0.006$
r_{11}^1	$-0.039 \pm 0.014 \pm 0.018$	$-0.033 \pm 0.013 \pm 0.009$
r_{00}^1	$-0.031 \pm 0.022 \pm 0.022$	$0.038 \pm 0.023 \pm 0.045$
$\text{Re}\{r_{10}^1\}$	$-0.020 \pm 0.011 \pm 0.007$	$-0.016 \pm 0.012 \pm 0.015$
r_{1-1}^1	$0.347 \pm 0.016 \pm 0.013$	$0.329 \pm 0.016 \pm 0.012$
$\text{Im}\{r_{10}^2\}$	$0.035 \pm 0.010 \pm 0.005$	$0.045 \pm 0.011 \pm 0.008$
$\text{Im}\{r_{1-1}^2\}$	$-0.353 \pm 0.016 \pm 0.018$	$-0.302 \pm 0.016 \pm 0.031$
r_{11}^5	$0.009 \pm 0.006 \pm 0.010$	$0.007 \pm 0.006 \pm 0.004$
r_{00}^5	$0.042 \pm 0.014 \pm 0.011$	$0.055 \pm 0.015 \pm 0.009$
$\text{Re}\{r_{10}^5\}$	$0.139 \pm 0.005 \pm 0.012$	$0.149 \pm 0.006 \pm 0.008$
r_{1-1}^5	$-0.006 \pm 0.008 \pm 0.007$	$-0.011 \pm 0.008 \pm 0.009$
$\text{Im}\{r_{10}^6\}$	$-0.128 \pm 0.005 \pm 0.006$	$-0.159 \pm 0.005 \pm 0.005$
$\text{Im}\{r_{1-1}^6\}$	$0.007 \pm 0.008 \pm 0.006$	$0.025 \pm 0.008 \pm 0.008$

Table 4: The 15 combinations of spin-density matrix elements r_{ik}^{04} , r_{ik}^α , as obtained from the BPC data in two Q^2 intervals. Statistical and systematic uncertainties are given separately. The data cover the kinematic range $0.25 < Q^2 < 0.85 \text{ GeV}^2$, $20 < W < 90 \text{ GeV}$, $0.6 < M_{\pi\pi} < 1.0 \text{ GeV}$ and $|t| < 0.6 \text{ GeV}^2$. The average Q^2 values for the two intervals are $\langle Q^2 \rangle = 0.32 \text{ GeV}^2$ and $\langle Q^2 \rangle = 0.54 \text{ GeV}^2$, respectively.

ZEUS 1995 (BPC)			
	$0 < t < 0.1 \text{ GeV}^2$	$0.1 < t < 0.25 \text{ GeV}^2$	$0.25 < t < 0.6 \text{ GeV}^2$
r_{00}^{04}	$0.261 \pm 0.014 \pm 0.017$	$0.273 \pm 0.020 \pm 0.016$	$0.339 \pm 0.029 \pm 0.027$
$\text{Re}\{r_{10}^{04}\}$	$0.029 \pm 0.009 \pm 0.012$	$0.042 \pm 0.012 \pm 0.006$	$0.047 \pm 0.017 \pm 0.024$
r_{1-1}^{04}	$-0.036 \pm 0.012 \pm 0.014$	$-0.034 \pm 0.015 \pm 0.018$	$-0.048 \pm 0.019 \pm 0.012$
r_{11}^1	$-0.026 \pm 0.013 \pm 0.018$	$-0.043 \pm 0.017 \pm 0.019$	$-0.054 \pm 0.022 \pm 0.021$
r_{00}^1	$0.023 \pm 0.020 \pm 0.034$	$-0.029 \pm 0.028 \pm 0.051$	$-0.071 \pm 0.045 \pm 0.086$
$\text{Re}\{r_{10}^1\}$	$-0.012 \pm 0.011 \pm 0.014$	$-0.032 \pm 0.014 \pm 0.018$	$-0.016 \pm 0.021 \pm 0.032$
r_{1-1}^1	$0.328 \pm 0.016 \pm 0.015$	$0.333 \pm 0.020 \pm 0.023$	$0.300 \pm 0.026 \pm 0.020$
$\text{Im}\{r_{10}^2\}$	$0.027 \pm 0.010 \pm 0.013$	$0.038 \pm 0.014 \pm 0.019$	$0.044 \pm 0.020 \pm 0.030$
$\text{Im}\{r_{1-1}^2\}$	$-0.329 \pm 0.016 \pm 0.025$	$-0.319 \pm 0.020 \pm 0.027$	$-0.285 \pm 0.030 \pm 0.030$
r_{11}^5	$0.001 \pm 0.006 \pm 0.008$	$0.012 \pm 0.008 \pm 0.004$	$0.021 \pm 0.010 \pm 0.014$
r_{00}^5	$0.026 \pm 0.012 \pm 0.025$	$0.070 \pm 0.020 \pm 0.009$	$0.117 \pm 0.027 \pm 0.050$
$\text{Re}\{r_{10}^5\}$	$0.137 \pm 0.005 \pm 0.011$	$0.152 \pm 0.007 \pm 0.012$	$0.144 \pm 0.010 \pm 0.014$
r_{1-1}^5	$-0.002 \pm 0.008 \pm 0.008$	$-0.012 \pm 0.010 \pm 0.008$	$-0.018 \pm 0.014 \pm 0.010$
$\text{Im}\{r_{10}^6\}$	$-0.144 \pm 0.005 \pm 0.009$	$-0.135 \pm 0.007 \pm 0.004$	$-0.121 \pm 0.011 \pm 0.022$
$\text{Im}\{r_{1-1}^6\}$	$0.012 \pm 0.008 \pm 0.008$	$0.007 \pm 0.010 \pm 0.007$	$0.009 \pm 0.015 \pm 0.014$

Table 5: The 15 combinations of spin-density matrix elements r_{ik}^{04} , r_{ik}^α , as obtained from the BPC data in three t intervals. Statistical and systematic uncertainties are given separately. The data cover the kinematic range $0.25 < Q^2 < 0.85 \text{ GeV}^2$, $20 < W < 90 \text{ GeV}$, $0.6 < M_{\pi\pi} < 1.0 \text{ GeV}$ and $|t| < 0.6 \text{ GeV}^2$. The average $|t|$ values for the three intervals are $\langle |t| \rangle = 0.04 \text{ GeV}^2$, $\langle |t| \rangle = 0.16 \text{ GeV}^2$ and $\langle |t| \rangle = 0.37 \text{ GeV}^2$, respectively.

ZEUS 1995 (BPC)															
	r_{00}^{04}	$\text{Re}\{r_{10}^{04}\}$	r_{1-1}^{04}	r_{11}^1	r_{00}^1	$\text{Re}\{r_{10}^1\}$	r_{1-1}^1	$\text{Im}\{r_{10}^2\}$	$\text{Im}\{r_{1-1}^2\}$	r_{11}^5	r_{00}^5	$\text{Re}\{r_{10}^5\}$	r_{1-1}^5	$\text{Im}\{r_{10}^6\}$	$\text{Im}\{r_{1-1}^6\}$
r_{00}^{04}	1.000														
$\text{Re}\{r_{10}^{04}\}$	0.079	1.000													
r_{1-1}^{04}	0.046	0.054	1.000												
r_{11}^1	0.101	0.011	0.584	1.000											
r_{00}^1	-0.159	-0.025	-0.062	-0.414	1.000										
$\text{Re}\{r_{10}^1\}$	-0.068	-0.508	-0.127	-0.039	0.043	1.000									
r_{1-1}^1	-0.327	-0.201	-0.082	-0.082	0.052	0.116	1.000								
$\text{Im}\{r_{10}^2\}$	0.105	0.445	0.075	0.062	-0.039	-0.293	-0.095	1.000							
$\text{Im}\{r_{1-1}^2\}$	0.312	0.097	0.019	0.009	-0.029	-0.069	0.073	0.072	1.000						
r_{11}^5	-0.095	0.231	0.014	-0.075	0.063	-0.038	0.014	0.011	0.050	1.000					
r_{00}^5	0.248	0.578	0.053	0.087	-0.223	-0.452	-0.150	0.544	0.133	-0.300	1.000				
$\text{Re}\{r_{10}^5\}$	0.299	0.080	-0.225	-0.138	-0.184	-0.201	-0.098	-0.084	0.023	-0.004	-0.044	1.000			
r_{1-1}^5	0.003	-0.325	0.052	0.058	0.007	0.117	-0.015	-0.012	-0.068	-0.479	-0.051	0.078	1.000		
$\text{Im}\{r_{10}^6\}$	-0.308	0.051	-0.359	-0.221	-0.356	0.031	0.009	-0.056	-0.057	0.044	0.034	0.056	-0.054	1.000	
$\text{Im}\{r_{1-1}^6\}$	-0.009	0.337	-0.046	-0.074	0.014	0.062	-0.072	0.169	0.035	0.443	0.041	-0.040	-0.251	0.055	1.000

Table 6: Correlation matrix for the 15 combinations of spin-density matrix elements r_{ik}^{04} , r_{ik}^{α} , as obtained from the BPC data.

ZEUS 1995 (DIS)															
	r_{00}^{04}	$\text{Re}\{r_{10}^{04}\}$	r_{1-1}^{04}	r_{11}^1	r_{00}^1	$\text{Re}\{r_{10}^1\}$	r_{1-1}^1	$\text{Im}\{r_{10}^2\}$	$\text{Im}\{r_{1-1}^2\}$	r_{11}^5	r_{00}^5	$\text{Re}\{r_{10}^5\}$	r_{1-1}^5	$\text{Im}\{r_{10}^6\}$	$\text{Im}\{r_{1-1}^6\}$
r_{00}^{04}	1.000														
$\text{Re}\{r_{10}^{04}\}$	-0.014	1.000													
r_{1-1}^{04}	0.020	-0.081	1.000												
r_{11}^1	0.061	-0.097	0.273	1.000											
r_{00}^1	-0.011	-0.042	0.070	-0.381	1.000										
$\text{Re}\{r_{10}^1\}$	0.086	-0.219	0.146	-0.056	-0.086	1.000									
r_{1-1}^1	-0.203	0.059	-0.060	-0.050	0.023	0.196	1.000								
$\text{Im}\{r_{10}^2\}$	0.017	0.176	0.013	-0.032	-0.061	0.152	0.099	1.000							
$\text{Im}\{r_{1-1}^2\}$	0.182	-0.008	-0.028	0.041	0.005	0.170	0.433	0.095	1.000						
r_{11}^5	-0.257	0.292	-0.050	-0.174	0.088	-0.038	-0.054	0.166	-0.086	1.000					
r_{00}^5	0.172	0.422	-0.027	0.067	-0.221	-0.333	-0.004	0.254	0.042	-0.279	1.000				
$\text{Re}\{r_{10}^5\}$	-0.131	0.331	-0.460	-0.170	-0.322	-0.221	0.023	-0.029	-0.162	0.054	-0.004	1.000			
r_{1-1}^5	0.015	-0.270	0.309	-0.022	-0.013	0.179	-0.107	0.195	-0.094	-0.156	-0.028	-0.038	1.000		
$\text{Im}\{r_{10}^6\}$	0.124	0.076	-0.432	-0.220	-0.339	-0.134	-0.143	-0.214	0.102	0.021	0.092	0.506	-0.014	1.000	
$\text{Im}\{r_{1-1}^6\}$	-0.071	0.244	0.109	-0.043	0.007	0.205	-0.045	0.284	-0.245	0.221	-0.002	0.001	0.286	0.013	1.000

Table 7: Correlation matrix for the 15 combinations of spin-density matrix elements r_{ik}^{04} , r_{ik}^{α} , as obtained from the DIS data.

ZEUS 1995 (BPC)		
	$0.6 < M_{\pi\pi} < 0.77 \text{ GeV}$	$0.77 < M_{\pi\pi} < 1.0 \text{ GeV}$
r_{00}^{04}	$0.311 \pm 0.014 \pm 0.013$	$0.227 \pm 0.018 \pm 0.016$
$\text{Re}\{r_{10}^{04}\}$	$0.026 \pm 0.009 \pm 0.010$	$0.032 \pm 0.010 \pm 0.005$
r_{1-1}^{04}	$-0.031 \pm 0.011 \pm 0.006$	$-0.062 \pm 0.014 \pm 0.010$
r_{11}^1	$-0.030 \pm 0.012 \pm 0.009$	$-0.054 \pm 0.015 \pm 0.007$
r_{00}^1	$0.020 \pm 0.019 \pm 0.042$	$-0.011 \pm 0.026 \pm 0.041$
$\text{Re}\{r_{10}^1\}$	$-0.007 \pm 0.010 \pm 0.010$	$-0.029 \pm 0.013 \pm 0.010$
r_{1-1}^1	$0.321 \pm 0.014 \pm 0.016$	$0.369 \pm 0.018 \pm 0.027$
$\text{Im}\{r_{10}^2\}$	$0.023 \pm 0.010 \pm 0.010$	$0.064 \pm 0.012 \pm 0.017$
$\text{Im}\{r_{1-1}^2\}$	$-0.302 \pm 0.014 \pm 0.029$	$-0.362 \pm 0.019 \pm 0.016$
r_{11}^5	$0.015 \pm 0.006 \pm 0.009$	$-0.002 \pm 0.007 \pm 0.006$
r_{00}^5	$0.026 \pm 0.013 \pm 0.019$	$0.077 \pm 0.015 \pm 0.017$
$\text{Re}\{r_{10}^5\}$	$0.152 \pm 0.005 \pm 0.008$	$0.129 \pm 0.007 \pm 0.012$
r_{1-1}^5	$-0.010 \pm 0.007 \pm 0.007$	$-0.009 \pm 0.009 \pm 0.013$
$\text{Im}\{r_{10}^6\}$	$-0.155 \pm 0.004 \pm 0.004$	$-0.125 \pm 0.006 \pm 0.006$
$\text{Im}\{r_{1-1}^6\}$	$0.019 \pm 0.007 \pm 0.006$	$0.007 \pm 0.009 \pm 0.008$

Table 8: The 15 combinations of spin-density matrix elements r_{ik}^{04} , r_{ik}^{α} , as obtained from the BPC data in two $M_{\pi\pi}$ intervals. Statistical and systematic uncertainties are given separately. The data cover the kinematic range $0.25 < Q^2 < 0.85 \text{ GeV}^2$, $20 < W < 90 \text{ GeV}$, $0.6 < M_{\pi\pi} < 1.0 \text{ GeV}$ and $|t| < 0.6 \text{ GeV}^2$.

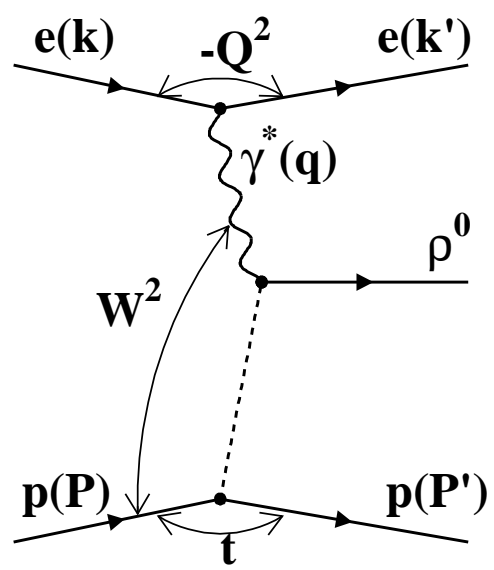


Figure 1: Schematic diagram of the reaction $ep \rightarrow e\rho^0 p$, indicating the kinematic variables used in this analysis.

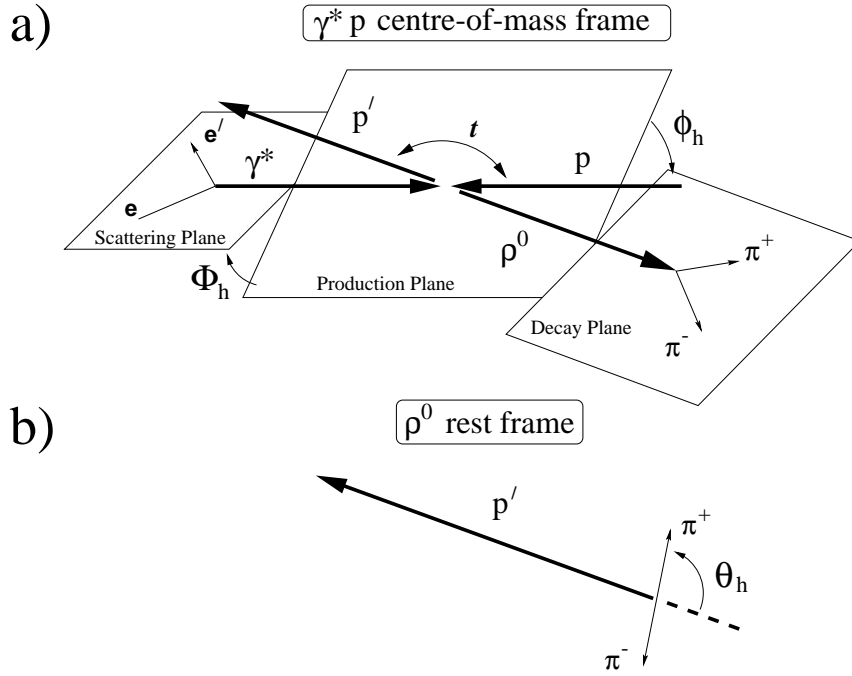


Figure 2: Schematic diagrams of (a) the process $ep \rightarrow e\rho^0 p$ in the $\gamma^* p$ centre-of-mass system, and (b) the decay of the ρ^0 in its rest frame. Three angles suffice to describe the reaction: the azimuthal angle between the scattering plane and the production plane, Φ_h ; and the two ρ^0 decay angles, ϕ_h , the azimuthal angle between the production and decay planes, defined in either the $\gamma^* p$ system or in the ρ^0 rest frame; and θ_h , which is the polar angle of the positively-charged decay product defined with respect to the direction of the ρ^0 momentum vector in the $\gamma^* p$ system, or, equivalently, the direction opposite to the momentum-vector of the final-state proton in the rest frame of the ρ^0 meson. This choice of the spin-quantisation axis defines the helicity frame.

ZEUS 1995

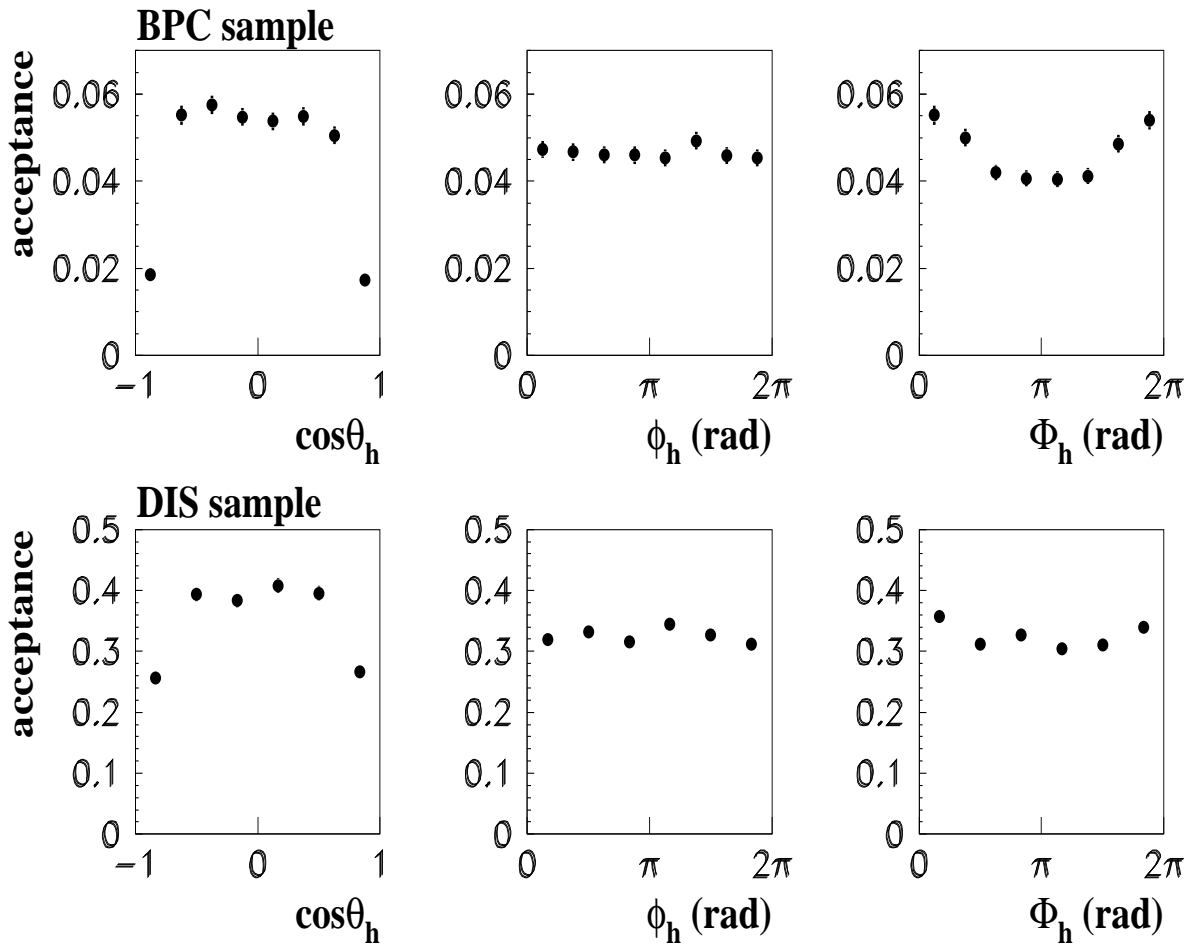


Figure 3: Acceptance as a function of $\cos \theta_h$, ϕ_h and Φ_h , for the BPC and the DIS data samples. The bars indicate the statistical uncertainties.

ZEUS 1995

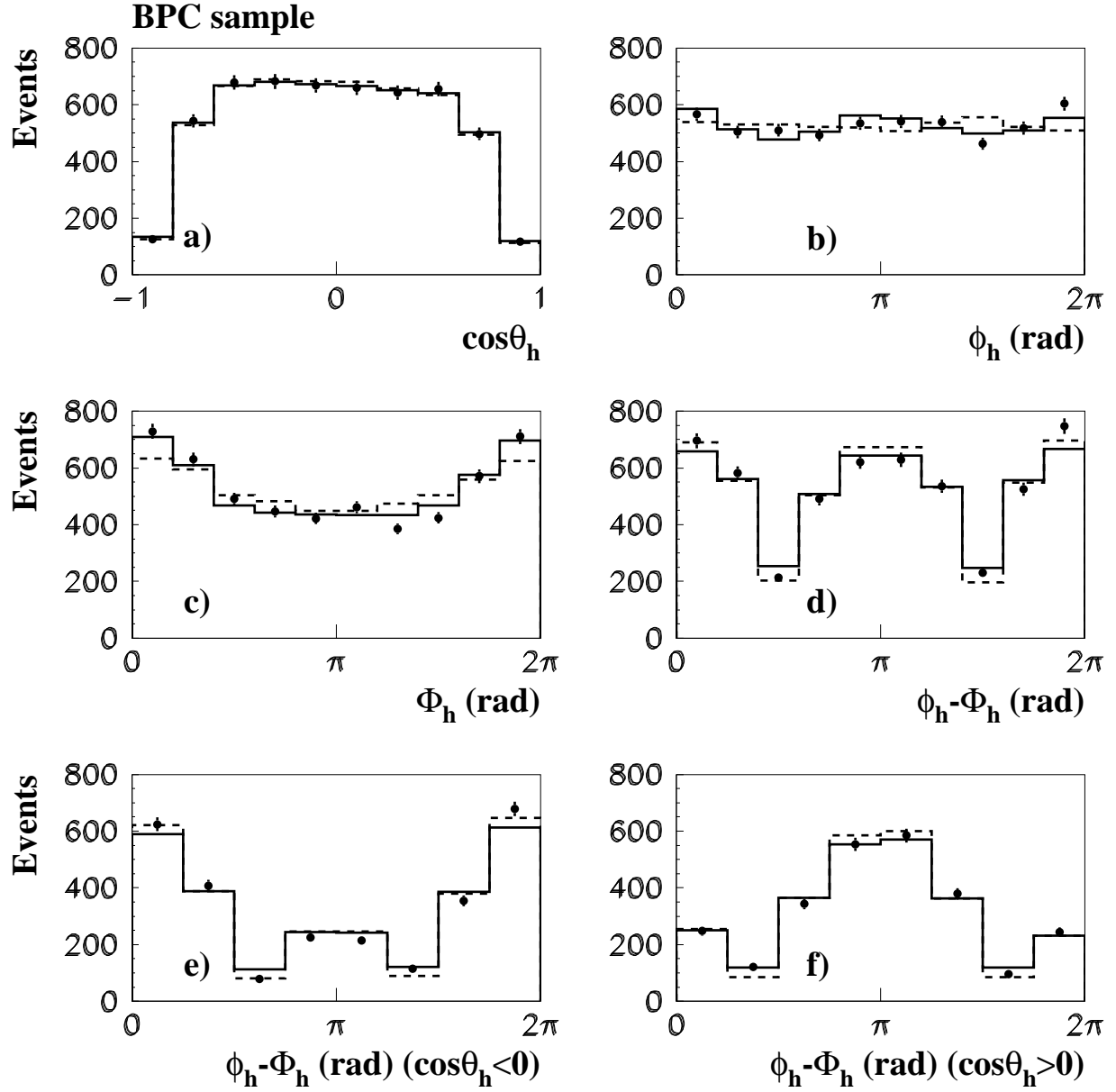


Figure 4: Observed distributions for $\cos\theta_h$ (a), ϕ_h (b), Φ_h (c) and $\psi_h = \phi_h - \Phi_h$ (d, e, f) of the reconstructed BPC data (points) and the reconstructed Monte Carlo events (histograms). The solid histograms correspond to the Monte Carlo data reweighted with Eq. (3), in which the results of the present analysis were used for the 15 combinations of matrix elements r_{ik}^{04} , r_{ik}^α . The dashed histograms correspond to the SHC hypothesis. The distributions are not corrected for acceptance. The error bars indicate the statistical uncertainty. The statistical uncertainty of the simulated distributions is negligible.

ZEUS 1995

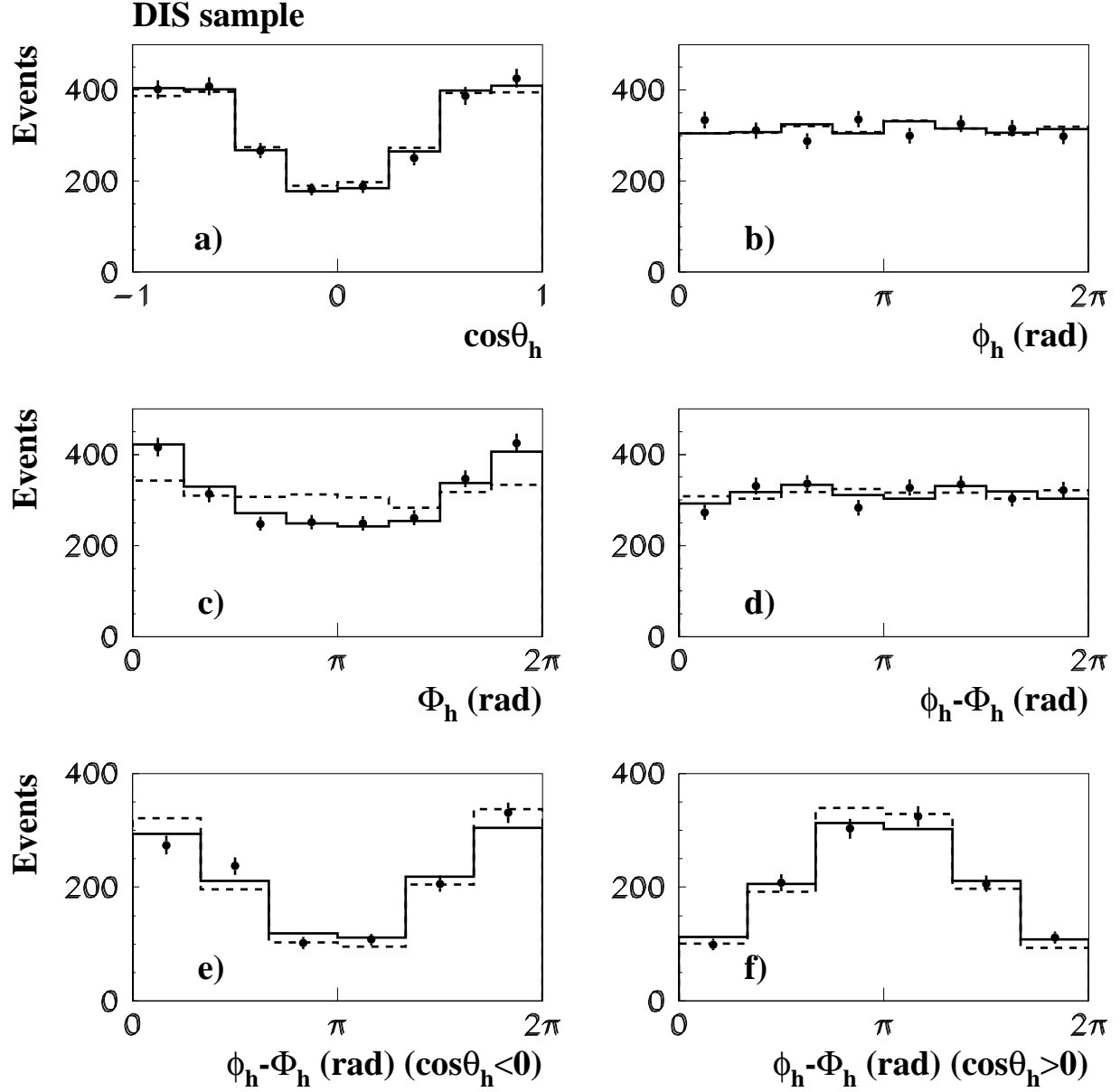


Figure 5: Observed distributions for $\cos\theta_h$ (a), ϕ_h (b), Φ_h (c) and $\psi_h = \phi_h - \Phi_h$ (d, e, f) of the reconstructed DIS data (points) and the reconstructed Monte Carlo events (histograms). The solid histograms correspond to the Monte Carlo data reweighted with Eq. (3), in which the results of the present analysis were used for the 15 combinations of matrix elements r_{ik}^{04} , r_{ik}^α . The dashed histograms correspond to the SHC hypothesis. The distributions are not corrected for acceptance. The error bars indicate the statistical uncertainty. The statistical uncertainty of the simulated distributions is negligible.

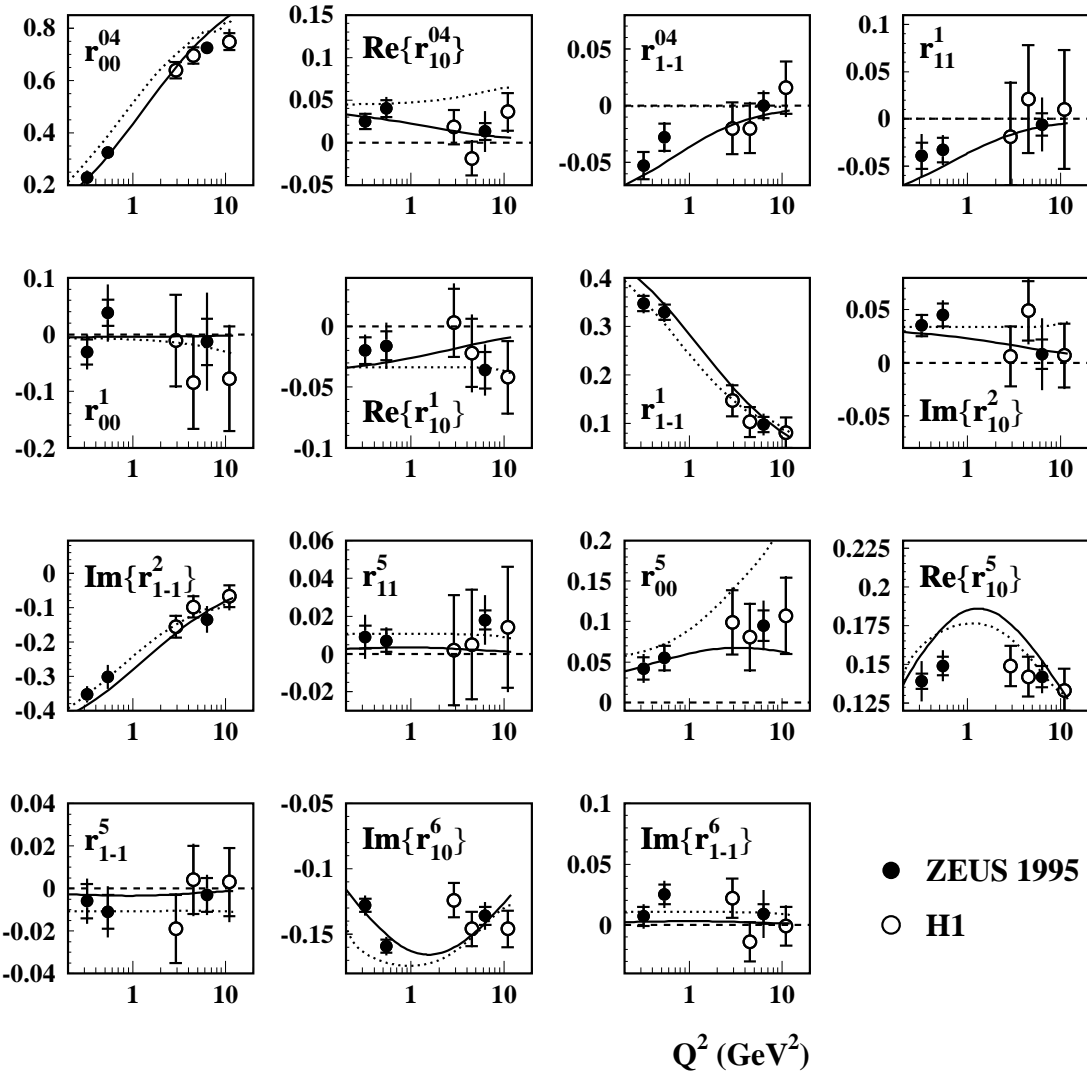


Figure 6: The 15 combinations of spin-density matrix elements r_{ik}^{04} , r_{ik}^{α} , as obtained from the BPC and DIS data sets as a function of Q^2 . The full symbols indicate the present results; the open points indicate the H1 results [10]. For the ZEUS points, the inner error bars indicate the statistical uncertainties, the outer the statistical and systematic uncertainties summed in quadrature. For the H1 points, the error bars indicate the quadratic sum of the statistical and systematic uncertainties. The continuous curves are the prediction of the model calculation of Ref. [20], the dotted curves the prediction of Ref. [21]. The dashed lines indicate the SCHC expectation. The predictions of Ref. [21] and of SCHC coincide for r_{1-1}^{04} and r_{11}^1 .

ZEUS 1995

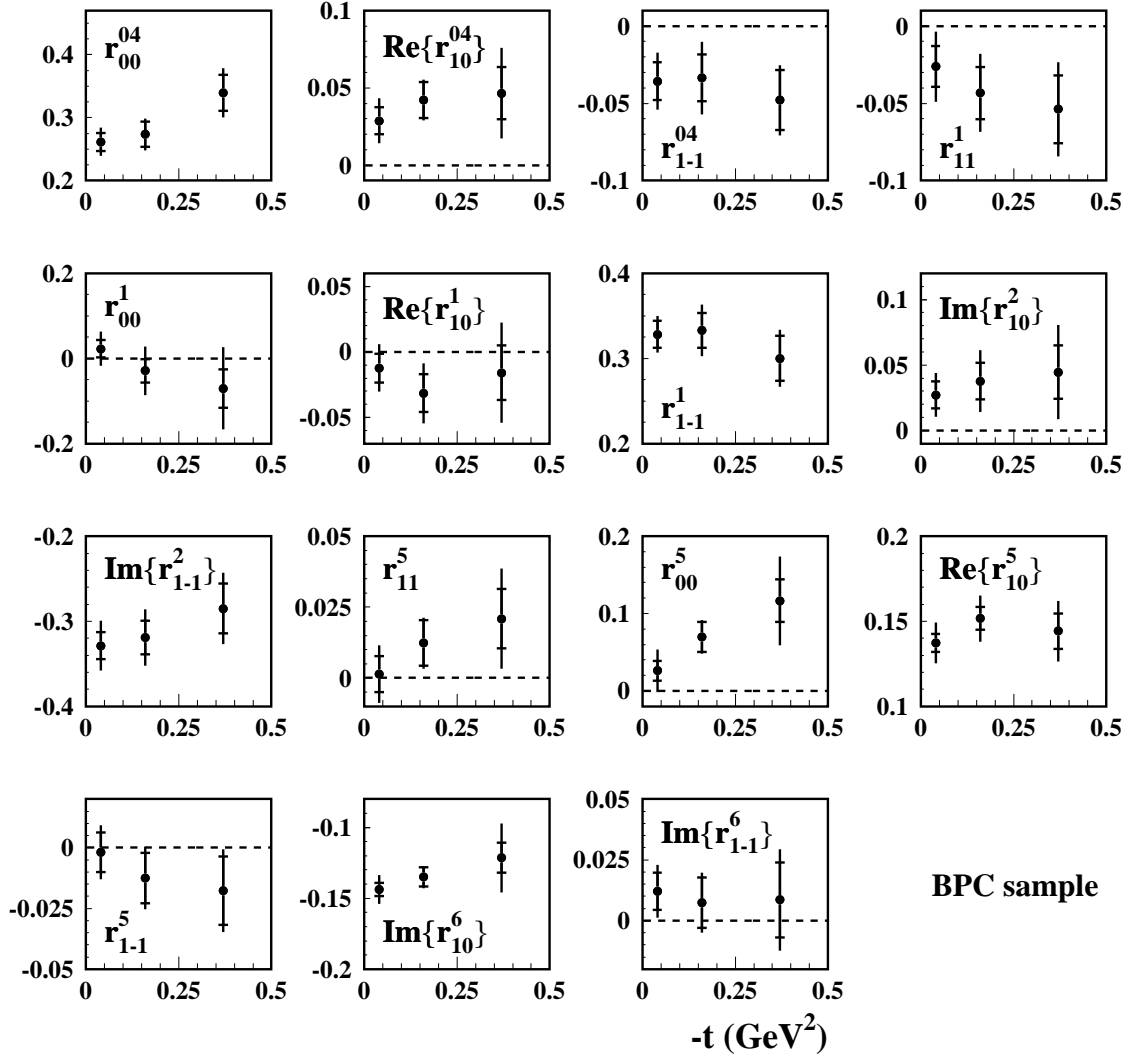


Figure 7: The 15 combinations of spin-density matrix elements r_{ik}^{04} , r_{ik}^{α} , as obtained from the BPC data as a function of t . The inner error bars indicate the statistical uncertainties, the outer bars the statistical and systematic uncertainties summed in quadrature. The horizontal bars indicate the size of the bins. The dashed lines indicate the prediction of SCHC, where available. The data cover the kinematic range $0.25 < Q^2 < 0.85$ GeV 2 , $20 < W < 90$ GeV, $0.6 < M_{\pi\pi} < 1.0$ GeV and $|t| < 0.6$ GeV 2 .

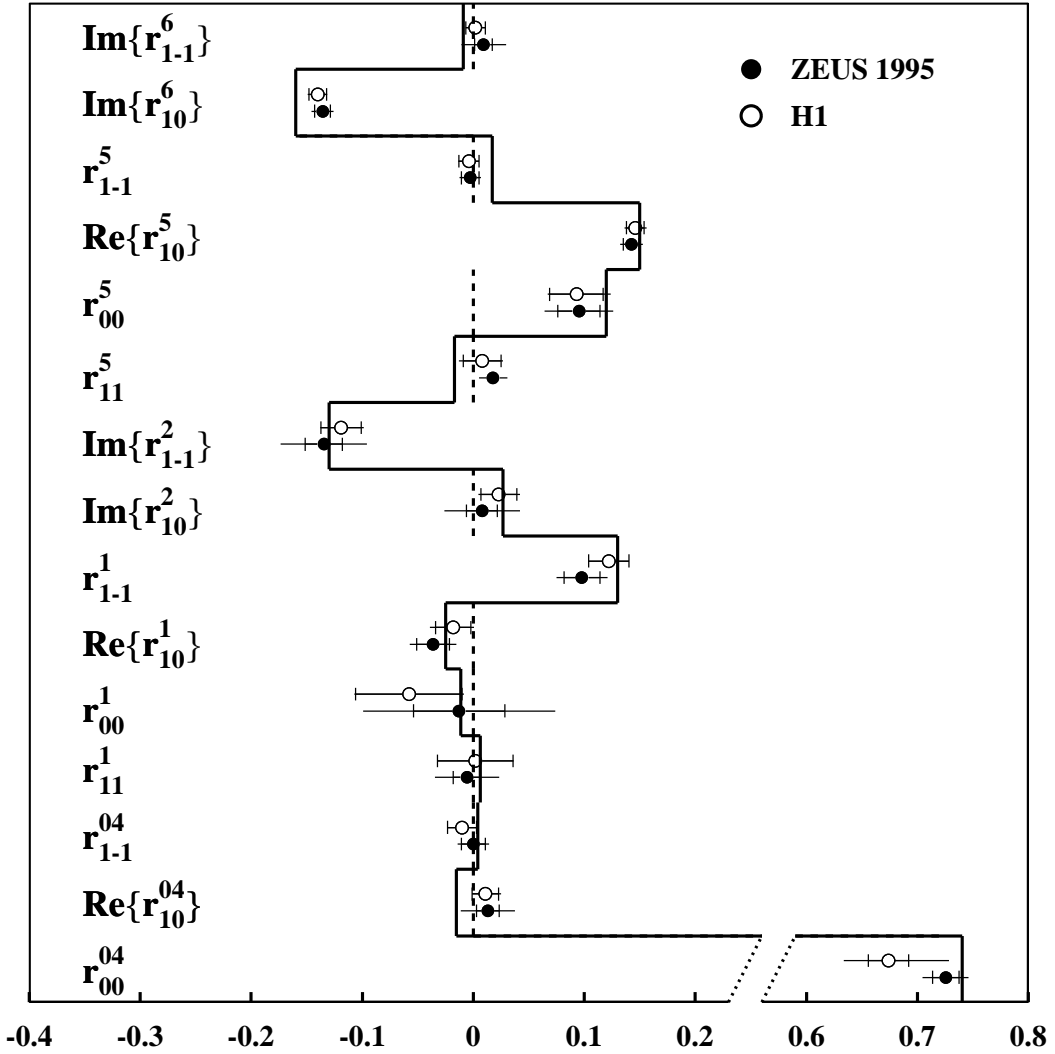


Figure 8: The 15 combinations of spin-density matrix elements r_{ik}^{04} , r_{ik}^{α} , as obtained from the DIS data compared with the predictions of the model calculation of Ref. [19] (continuous histogram) and of SCHC (dashed histogram, see text for details). The solid points indicate the present results; the open points indicate the H1 data [10]. The inner error bars indicate the statistical uncertainties, the outer the statistical and systematic uncertainties summed in quadrature. The ZEUS data cover the kinematic range $3 < Q^2 < 30 \text{ GeV}^2$ ($\langle Q^2 \rangle = 6.3 \text{ GeV}^2$), $40 < W < 120 \text{ GeV}$ ($\langle W \rangle = 73 \text{ GeV}$), $0.6 < M_{\pi\pi} < 1.0 \text{ GeV}$ and $|t| < 0.6 \text{ GeV}^2$. The H1 data cover the range $1 < Q^2 < 60 \text{ GeV}^2$, $30 < W < 140 \text{ GeV}$ and $|t| < 0.5 \text{ GeV}^2$. The prediction of Ref. [19] is for $Q^2 = 10 \text{ GeV}^2$ and $W = 100 \text{ GeV}$.